

Advanced Healthcare Materials

Graphene Oxide-doped Gellan Gum-PEGDA hydrogel mimicking the mechanical and lubrication properties of articular cartilage

--Manuscript Draft--

Manuscript Number:	adh.m.202001434		
Article Type:	Full Paper		
Corresponding Author:	Diego Trucco Scuola Superiore Sant'Anna Pisa, Italy ITALY		
Corresponding Author E-Mail:	diego.trucco@santannapisa.it		
Order of Authors:	Diego Trucco, MSc Lorenzo Vannozzi Eti Teblum Madina Telkhozhayeva Gilbert Daniel Nessim Saverio Affatato Hind Al-Haddad Gina Lisignoli Leonardo Ricotti		
Keywords:	Cartilage mechanical properties; Cartilage lubrication properties; Hydrogels; Gellan gum; Graphene Oxide		
Section/Category:			
Abstract:	<p>Articular cartilage (AC) is a specialized connective tissue able to provide a low-friction gliding surface supporting shock-absorption, reducing stresses, and guaranteeing wear-resistance thanks to its structure and mechanical and lubrication properties. Being an avascular tissue, AC has a limited ability to heal defects. Nowadays, conventional strategies show several limitations, thus resulting limited in properly restoring chondral defects. Several tissue engineering approaches have been proposed to restore the AC's native properties without reproducing its mechanical and lubrication properties yet.</p> <p>This work reports the fabrication of a bilayered structure made of gellan gum (GG) and poly (ethylene glycol) diacrylate (PEGDA), able to mimic the mechanical and lubrication features of both AC superficial and deep zones. Through appropriate combinations of GG and PEGDA, cartilage Young's modulus was effectively mimicked for both zones. Graphene oxide was used as a dopant agent for the superficial hydrogel layer, demonstrating a lower friction than the non-doped counterpart. The bilayered hydrogel's anti-wear properties were confirmed by using a knee simulator, following ISO 14243. Finally, in vitro tests with human chondrocytes confirmed the absence of cytotoxicity effects.</p> <p>The results shown in this paper open the way to a multilayered synthetic injectable or surgically implantable filler for restoring AC defects.</p>		
Suggested Reviewers:	Sourabh Ghosh Indian Institute of Technology Delhi sghosh08@textile.iitd.ac.in	Toshinori Fujie Tokyo Institute of Technology t_fujie@bio.titech.ac.jp	Richard van Arkel Imperial College London r.vanarkel@imperial.ac.uk

	Jonathan R.T. Jeffers Imperial College London j.jeffers@imperial.ac.uk
	Sumi Lee Jeonbuk Institute sumilee@jbnu.ac.kr
	Lorenzo Moroni Maastricht University l.moroni@maastrichtuniversity.nl
Opposed Reviewers:	
Author Comments:	
Additional Information:	
Question	Response
Please submit a plain text version of your cover letter here.	<p>Dear Editor,</p> <p>We would like to submit our paper entitled “Graphene Oxide-doped Gellan Gum-PEGDA hydrogel mimicking the mechanical and lubrication properties of articular cartilage” to be considered for publication in the prestigious journal Advanced Healthcare Materials.</p> <p>The paper provides an original contribution to the field of nanocomposite materials applied for the cartilage tissue engineering, a domain that is receiving a growing attention.</p> <p>In the paper, we present a possible new strategy to repair chondral defects by mimicking the mechanical-zone specific and lubrication properties of the articular cartilage tissue, combining gellan gum (GG), poly (ethylene glycol)-diacrylate (PEGDA) and graphene oxide (GO). The results reported in the manuscript highlight the potential use of a multilayered synthetic injectable or surgically implantable filler for restoring AC defects. We believe these findings will be of interest to the readers of your journal.</p> <p>The challenges addressed by this paper stand at the interface between biomedical science and materials engineering, thus we think the paper has the potential to raise the interest of a large pool of scientists working in these domains.</p> <p>We declare that this manuscript (or any part of it) is original, has not been published before and is not currently being considered for publication elsewhere.</p> <p>As Corresponding Author, I confirm that this manuscript has been read and approved for submission by all the named authors.</p> <p>Please let me know of your decision at your earliest convenience.</p> <p>Thank you in advance for your time and consideration.</p> <p>Yours sincerely,</p> <p>Diego Trucco, PhD student in BioRobotics, The BioRobotics Institute, Scuola Superiore Sant’Anna Viale Rinaldo Piaggio, 34 – 56025 Pontedera (Pisa), Italy Tel: +39 050 883020 - Fax: +39 050 883101 E-Mail: diego.trucco@santannapisa.it</p>
Does the research described in this manuscript include animal experiments?	No
Does the research described in this manuscript include human research participants (including for experiments with sensors or wearable technologies) or	Yes

tissue samples from human subjects (including blood or sweat)?	
<p>Please confirm that informed written consent from all participants or next of kin was obtained prior to the research, and that this is included in the Experimental section of your manuscript.</p> <p>as follow-up to "Does the research described in this manuscript include human research participants (including for experiments with sensors or wearable technologies) or tissue samples from human subjects (including blood or sweat)?"</p>	Yes, I confirm
<p>If required, please confirm that approval from a national or institutional ethics board/committee was obtained prior to the research, and that this is included in the Experimental section of your manuscript.</p> <p>as follow-up to "Does the research described in this manuscript include human research participants (including for experiments with sensors or wearable technologies) or tissue samples from human subjects (including blood or sweat)?"</p>	Yes, I confirm
<p>Please provide the name of the ethics board/committee giving the approval in the textbox below, as well as in the Experimental section of your manuscript.</p> <p>as follow-up to "If required, please confirm that approval from a national or institutional ethics board/committee was obtained prior to the research, and that this is included in the Experimental section of your manuscript."</p>	Istituto Ortopedico Rizzoli's ethics board
<p>Please provide the assigned study/project number in the textbox below, as well as in the Experimental section of your manuscript.</p> <p>as follow-up to "If required, please confirm that approval from a national or institutional ethics board/committee was obtained prior to the research, and that this is included in the Experimental section of your manuscript."</p>	814413
Do you or any of your co-authors have a conflict of interest to declare?	No. The authors declare no conflict of interest.



Scuola Superiore
Sant'Anna

Pisa, August 03, 2020

Dear Editor,

We would like to submit our paper entitled "*Graphene Oxide-doped Gellan Gum-PEGDA hydrogel mimicking the mechanical and lubrication properties of articular cartilage*" to be considered for publication in the prestigious journal *Advanced Healthcare Materials*.

The paper provides an original contribution to the field of nanocomposite materials applied for the cartilage tissue engineering, a domain that is receiving a growing attention.

In the paper, we present a possible new strategy to repair chondral defects by mimicking the mechanical-zone specific and lubrication properties of the articular cartilage tissue, combining gellan gum (GG), poly (ethylene glycol)-diacrylate (PEGDA) and graphene oxide (GO). The results reported in the manuscript highlight the potential use of a multilayered synthetic injectable or surgically implantable filler for restoring AC defects. We believe these findings will be of interest to the readers of your journal.

The challenges addressed by this paper stand at the interface between biomedical science and materials engineering, thus we think the paper has the potential to raise the interest of a large pool of scientists working in these domains.

We declare that this manuscript (or any part of it) is original, has not been published before and is not currently being considered for publication elsewhere.

As Corresponding Author, I confirm that this manuscript has been read and approved for submission by all the named authors.

Please let me know of your decision at your earliest convenience.

Thank you in advance for your time and consideration.

Yours sincerely,

Diego Trucco,

PhD student in BioRobotics,

The BioRobotics Institute, Scuola Superiore Sant'Anna

Viale Rinaldo Piaggio, 34 – 56025 Pontedera (Pisa), Italy

Tel: +39 050 883020 - Fax: +39 050 883101

E-Mail: diego.trucco@santannapisa.it



Graphene Oxide-doped Gellan Gum-PEGDA hydrogel mimicking the mechanical and lubrication properties of articular cartilage

Diego Trucco^{†,*}, Lorenzo Vannozzi[†], Eti Teblum, Madina Telkhozhayeva, Gilbert Daniel Nessim, Saverio Affatato, Hind Al-Haddad, Gina Lisignoli[§] and Leonardo Ricotti[§]

D. Trucco, Dr. L. Vannozzi, Hind Al-Haddad, Prof. L. Ricotti
The BioRobotics Institute, Scuola Superiore Sant'Anna,
Piazza Martiri della Libertà 33, 56127 Pisa, Italy

Department of Excellence in Robotics & AI, Scuola Superiore Sant'Anna,
Piazza Martiri della Libertà 33, 56127 Pisa, Italy

E-mail: diego.trucco@santannapisa.it

E-mail: leonardo.ricotti@santannapisa.it

D. Trucco, Dr. G. Lisignoli
IRCSS Istituto Ortopedico Rizzoli,
SC Laboratorio di Immunoreumatologia e Rigenerazione Tissutale,
Via di Barbiano, 1/10, Bologna 40136, Italy

E-mail: gina.lisignoli@ior.it

Dr. E. Teblum, M. Telkhozhayeva, Prof. Gilbert D. Nessim,
Department of Chemistry, Bar-Ilan University,
Ramat Gan 52900, Israel

Bar Ilan Institute for Nanotechnology and Advanced Materials (BINA),
Bar-Ilan University, Ramat Gan 52900, Israel

Dr. S. Affatato
IRCSS Istituto Ortopedico Rizzoli,
Laboratorio Tecnologie Biomediche,
Via di Barbiano, 1/10, Bologna 40136, Italy

[†] equally contributing authors

* Corresponding Author

§ Co-corresponding Authors

Keywords: Cartilage substitute, Cartilage mechanical properties, Cartilage lubrication properties, Hydrogels, Gellan gum, Polyethylene glycol diacrylate, Graphene Oxide

Articular cartilage (AC) is a specialized connective tissue able to provide a low-friction gliding surface supporting shock-absorption, reducing stresses, and guaranteeing wear-resistance thanks to its structure and mechanical and lubrication properties. Being an avascular tissue, AC has a limited ability to heal defects. Nowadays, conventional strategies show several limitations, thus resulting limited in properly restoring chondral defects. Several tissue engineering approaches have been proposed to restore the AC's native properties without reproducing its mechanical and lubrication properties yet.

This work reports the fabrication of a bilayered structure made of gellan gum (GG) and poly(ethylene glycol) diacrylate (PEGDA), able to mimic the mechanical and lubrication features of both AC superficial and deep zones. Through appropriate combinations of GG and PEGDA, cartilage Young's modulus was effectively mimicked for both zones. Graphene oxide was used as a dopant agent for the superficial hydrogel layer, demonstrating a lower friction than the non-doped counterpart. The bilayered hydrogel's anti-wear properties were confirmed by using a knee simulator, following ISO 14243. Finally, *in vitro* tests with human chondrocytes confirmed the absence of cytotoxicity effects.

The results shown in this paper open the way to a multilayered synthetic injectable or surgically implantable filler for restoring AC defects.

1. Introduction

Cartilage is a specialized avascular and aneural connective tissue capable of bearing mechanical stresses without permanent distortion. Three types of cartilage tissue (elastic, fibrocartilage and hyaline) are distributed in different parts of the human body, designated to perform specific functions depending on their structural composition.^[1] In particular, hyaline cartilage, also named articular cartilage (AC), is the most common type of cartilage that is present in hips,

1 elbows, shoulders and knee joints. It covers the opposing bone surfaces within each joint,
2 providing a low-friction gliding surface for the articulation supporting shock-absorption,
3
4 distributing loads, reducing stresses on the subchondral bone, and guaranteeing wear-
5
6 resistance.^[2]
7

8
9 AC is an anisotropic and viscoelastic tissue. From a functional and structural viewpoint, it can
10
11 be divided into four zones, which vary in extracellular matrix (ECM) composition, density,
12
13 collagen fibers assembling, phenotype and chondrocyte activity.^[2b, 3] The superficial zone, also
14
15 named the tangential zone, is in direct contact with the synovial fluid of the joint. It is composed
16
17 of elongated chondrocytes, present with high density and organized parallel to the articular
18
19 surface.^[4] This layer provides the smooth gliding surface guaranteeing lubrication and low wear
20
21 of the joint, exhibiting a lower tensile strength and stiffness than the deeper zones in terms of
22
23 compressive properties.^[2b] The middle zone, also named transitional zone between superficial
24
25 and deep ones, is featured by a low density of spherical-shaped chondrocytes and collagen
26
27 fibrils loosely packed and obliquely aligned to the articular surface. This zone guarantees the
28
29 resistance to compression forces due to the presence of thicker collagen fibers. The deep zone,
30
31 also termed radial zone, possesses spherical-shaped chondrocytes in a columnar fashion parallel
32
33 to the collagen fibers and perpendicular to the joint axis. This zone represents the bridge
34
35 between cartilage and bone and provides the highest resistance to compressive forces during
36
37 the movement of the joint. Finally, separated by a tidemark line and featured by the lowest
38
39 density of chondrocytes, the calcified zone represents the last layer of AC that, functionally,
40
41 anchors the cartilage to the bone^[2b]. However, overall, the AC can be considered divided in two
42
43 macro-regions: a superficial and a deep one.
44
45
46
47
48
49
50
51

52
53 The mechanical properties of AC differ from layer to layer.^[5] In particular, the compression
54
55 Young's modulus is in the range of 280 ± 160 kPa to 730 ± 260 kPa for the superficial and deep
56
57 regions, respectively. This is mainly due to their different permeability to the synovial fluid
58
59
60
61

1 flow.^[6] Overall, compression tests performed on the human knee AC exhibited a full-thickness
2 compression Young's modulus of 581 ± 168 kPa.^[5, 6b, 7]

3
4 Lubrication is another crucial property of AC. The superficial zone of AC provides a low-
5 friction gliding surface for the synovial joint, due to an extremely low coefficient of friction
6
7 between cartilage and cartilage (0.001 – 0.03)^[6b]. However, damages to the superficial area may
8
9 lead to a rapid wearing of AC and subsequent cartilage breakdown.^[4]

10
11
12 AC damages constitute the most common injuries of the knee joints.^[8] At the origin of the
13
14 damage, there are mechanical injuries (*i.e.*, adventitious or sport-related traumas)^[9] or age-
15
16 related degeneration (*i.e.*, osteoarthritis (OA)). However, also risk factors such as obesity and
17
18 genetic predisposition increase the probability to incur in a progressive AC degeneration.^[10]

19
20
21 Two types of defects can mainly occur: chondral (partial and full-thickness) and osteochondral
22
23 defects.^[9a, 11] Chondral defects only affect AC and do not extend to the underlying subchondral
24
25 bone, while osteochondral lesions involve both cartilage and the subchondral bone.^[12] In
26
27 osteochondral injuries, blood cells and mesenchymal progenitor cells have access to the
28
29 damaged cartilage from the subchondral bone, and the healing process leads to the formation
30
31 of weaker fibrous cartilage.^[9c] Differently, chondral defects cannot self-regenerate at all.
32
33
34 Conventional strategies, such as auto-, allo-, and xeno-grafts or joint replacement full implants,
35
36 have been adopted for cartilage repair, showing several limitations:^[13] osteochondral autografts,
37
38 which derive from lighter-load-bearing areas of the patient's joint, suffers from limited
39
40 availability and risk of donor site morbidity;^[14] limitations of osteochondral allograft
41
42 transplantation include low supply, short shelf-life and the need to find a fresh *post-mortem*
43
44 tissue from a very young donor;^[14b] osteochondral xenografts might show an immunogenic
45
46 response;^[15] prostheses, necessary in case of irreparable AC damage, must be implanted via
47
48 invasive surgery and the post-intervention recovery is long and complicated. In addition, the
49
50
51
52
53
54
55
56
57
58
59
60
61
62
63
64
65

1
2
3
4
5
6
7
8
9
10
11
12
13
14
15
16
17
18
19
20
21
22
23
24
25
26
27
28
29
30
31
32
33
34
35
36
37
38
39
40
41
42
43
44
45
46
47
48
49
50
51
52
53
54
55
56
57
58
59
60
61
62
63
64
65

eventual migration of prosthetic components or the loosening of implants frequently result in adjacent healthy tissue damage and, in some cases, in the need for a new surgery.^[9c]

Tissue engineering (TE) approaches have evolved to restore damaged native tissues by targeting the development of tissue substitutes *in vitro*.^[16] Commonly, such a process involves the combination of proper biomaterials, stem cells and growth factors that make up the main elements of three-dimensional (3D) engineered constructs. Scaffolds with a precise micro-architecture can support cell growth and the production of new ECM and, in the meantime, degrade to let the formation of the targeted biological tissue.^[17] However, many TE approaches exhibit limitations in terms of clinical translation, due to their relative inefficiency in re-establishing and mimicking the native tissue structure. In particular, it is difficult to reproduce the mechanical properties of the hyaline cartilage *in vitro* and, at the same time, to provide the scaffold with appropriate lubrication properties and let the scaffold degrade overtime without affecting such properties.^[18]

Multilayer structures were developed to regenerate osteochondral defects, which were composed of subchondral and cartilage zones.^[19] Osteochondral structures typically show poor mechanical properties and low cell differentiation in the bone and chondral direction, thus resulting relatively ineffective in repairing the defects and in restoring the native tissue. It is not straightforward, with TE approaches, to reconstitute a multilayer structure featured by mechanical properties reflecting the ones of the natural cartilage.^[20] Furthermore, TE constructs have to deal with a complex regulatory pathway before entering the clinics, being advanced therapy medicinal products bearing human cells. Fully synthetic (acellular) materials have the advantage of a simpler certification pathway, in addition to the fact that mechanical properties can be varied with higher flexibility, since cells are not embedded in the material and there is no need to keep them alive through a highly porous and soft environment.

1 Thus, synthetic acellular biomaterials can represent a valid alternative for the repair of cartilage
2 defects and the restoration of tissue functionalities and anatomical structures.^[16a] The
3
4 achievement of multilayered structures mimicking the zone-specific mechanical and lubrication
5
6 properties of the AC would be highly promising for AC repair.^[21] This approach can be used to
7
8 produce a kind of hemiarthroplasty, such as common metal substitutes, that could reconstitute
9
10 *in situ* the AC surface and also its overall mechanical properties.
11
12

13
14 Hydrogels are water-swollen materials that can be considered optimal candidates for being
15
16 injected or placed in the joint and to form 3D structures *in situ*.^[22] In the state-of-the-art, some
17
18 materials such as poly(ethylene oxide terephthalate)/poly-(butylene terephthalate)
19
20 (PEOT/PBT)^[23], poly(ϵ -caprolactone) (PCL)^[24], collagen^[25], chondroitin sulphate (CS) and
21
22 gelatin (G) microribbon (μ RB)^[20], have been shaped in multi-layers and proposed as possible
23
24 synthetic grafts for AC repair. However, none of them effectively mimicked both the
25
26 mechanical and lubrication properties of native cartilage. Thus, further efforts are needed in
27
28 this field.
29
30
31

32
33 Gellan gum (GG) is a water-soluble anionic polysaccharide produced by the bacterium
34
35 *Sphingomonas elodea*; the repeating unit of the polymer is a tetrasaccharide, which consists of
36
37 two residues of D-glucose and one of each residue of L-rhamnose and D-glucuronic acid.^[26]
38
39 GG has been widely studied in the TE field because of its properties such as biocompatibility,
40
41 biodegradability and ductility. In particular, its use has been particularly advantageous for the
42
43 cartilage TE field because of its structural similarity with native AC glycosaminoglycans due
44
45 to the presence of glucuronic acid residues in its repeating unit.^[19c, 27] This material is
46
47 thermosensitive and can be ionically crosslinked, interacting with monovalent and divalent ions,
48
49 producing hard and translucent gels in the presence of metallic ions, including sodium, calcium
50
51 and magnesium ones.^[27a, 28] GG has many advantages over other hydrogels, including shear-
52
53 thinning properties and gel formation at physiological temperatures, which make it a qualified
54
55
56
57
58
59
60
61
62
63
64
65

1 candidate for being injected into cartilage defects. However, the mechanical properties of such
2 a hydrogel are far from those related to the target cartilage zones.^[29]
3

4 In this paper, we explored the addition of poly (ethylene glycol) diacrylate (PEGDA) to improve
5 both stiffness and toughness of GG. PEGDA is a synthetic polymer used as a prepolymer
6 solution for the formation of a crosslinked polymeric network upon light exposure and the
7 presence of a photo-initiator.^[30] The combination of GG and PEGDA allows playing with both
8 noncovalent and covalent crosslinking methods, to achieve an interpenetrated polymeric
9 network able to effectively recover its shape after loading, as well as to show adequate
10 compressive strength. As mentioned, the achievement of optimal lubrication properties is also
11 a significant challenge, which is needed to improve the performance of the cartilage substitutes.
12

13 Carbon-based nanomaterials have been used in the literature to improve the mechanical and
14 electrical properties of bare materials. Recently, graphene oxide (GO) has been claimed as an
15 ideal nanomaterial for cartilage TE due to its chondro-inductive properties when embedded into
16 polymeric formulations. In fact, GO can provide a cell-friendly microenvironment able to
17 enhance chondrogenic differentiation.^[31] On the other hand, GO exhibits peculiar self-
18 lubricating and anti-wear properties,^[32] thanks to a high surface-to-volume ratio, a low effective
19 threshold resulting from its nanometer dimensions, which leads to optimizing the performance
20 of polymer composites.^[33]
21

22 We hypothesize that, by combining GG, PEGDA and GO, we could be able to develop a
23 bilayered hydrogel well mimicking both the mechanical features and the lubrication properties
24 of native AC. Such a nanocomposite hydrogel could be used as an injectable filler or a
25 surgically implantable substitute in chondral defects (Figure 1) showing no cytotoxicity and
26 guaranteeing suitable resistance to wear.
27
28
29
30
31
32
33
34
35
36
37
38
39
40
41
42
43
44
45
46
47
48
49
50
51
52
53
54
55
56
57
58
59
60
61
62
63
64
65

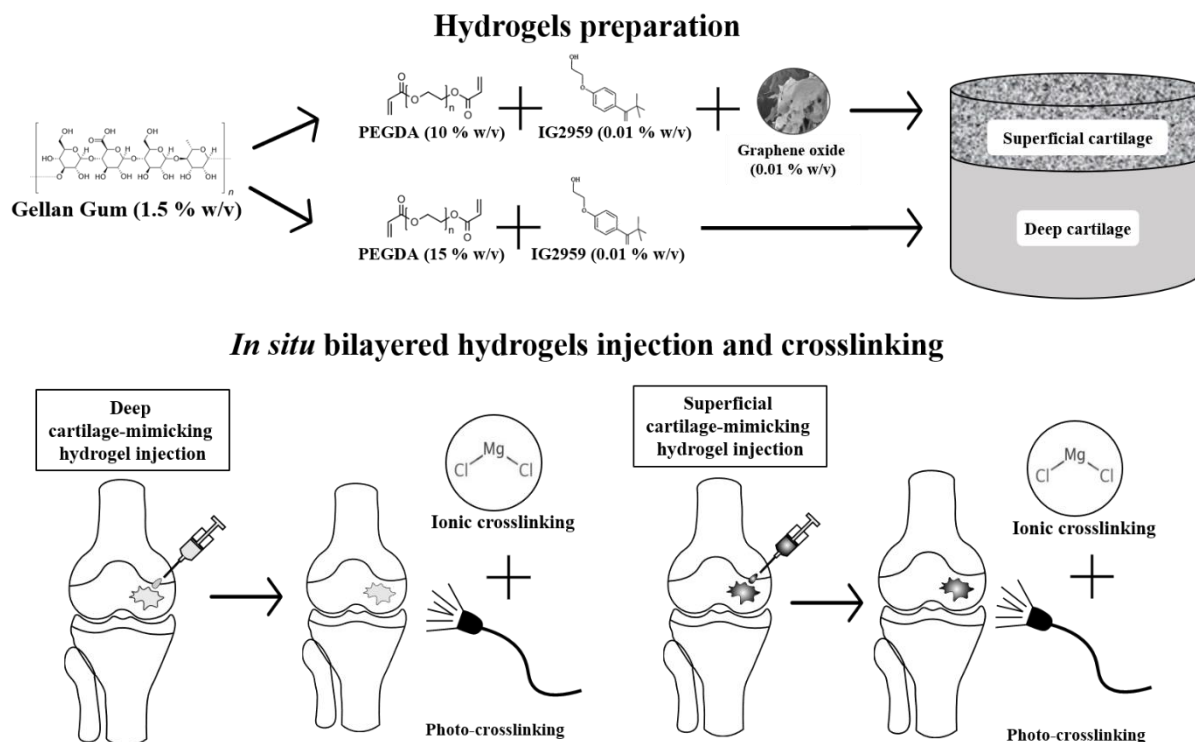


Figure 1. Depiction of the concept targeted in this work. By combining GG, PEGDA and GO, two hydrogels with specific properties, mimicking the ones of superficial and deep cartilage, respectively, are formulated. Then, the superficial and deep cartilage-mimicking hydrogels could be injected in situ and sequentially crosslinked using UV light (photo-crosslinking) and CaCl_2 solution (ionic crosslinking).

2. Results and discussion

2.1 Mechanical properties and swelling ratio

All combinations of GG and PEGDA at different concentrations and crosslinking approaches presented in the following are summarized in Table S1. Figure 2 reports the results of the mechanical characterization of hydrogels combining GG and PEGDA at different concentrations, aimed at mimicking the superficial and deep cartilage. Data show a relevant increase in the Young's modulus when PEGDA concentration increased from 10 (GG/PEGDA10) to 15 (GG/PEGDA15) % w/v. This range of values was then compared with the mechanical properties of superficial and deep cartilage, featured by a Young's modulus of 280 ± 160 kPa and 730 ± 260 kPa, respectively.^[6b] The first layer included the superficial and

the middle zones areas of a healthy cartilage, whereas the second layer included the deep zone of a healthy cartilage.

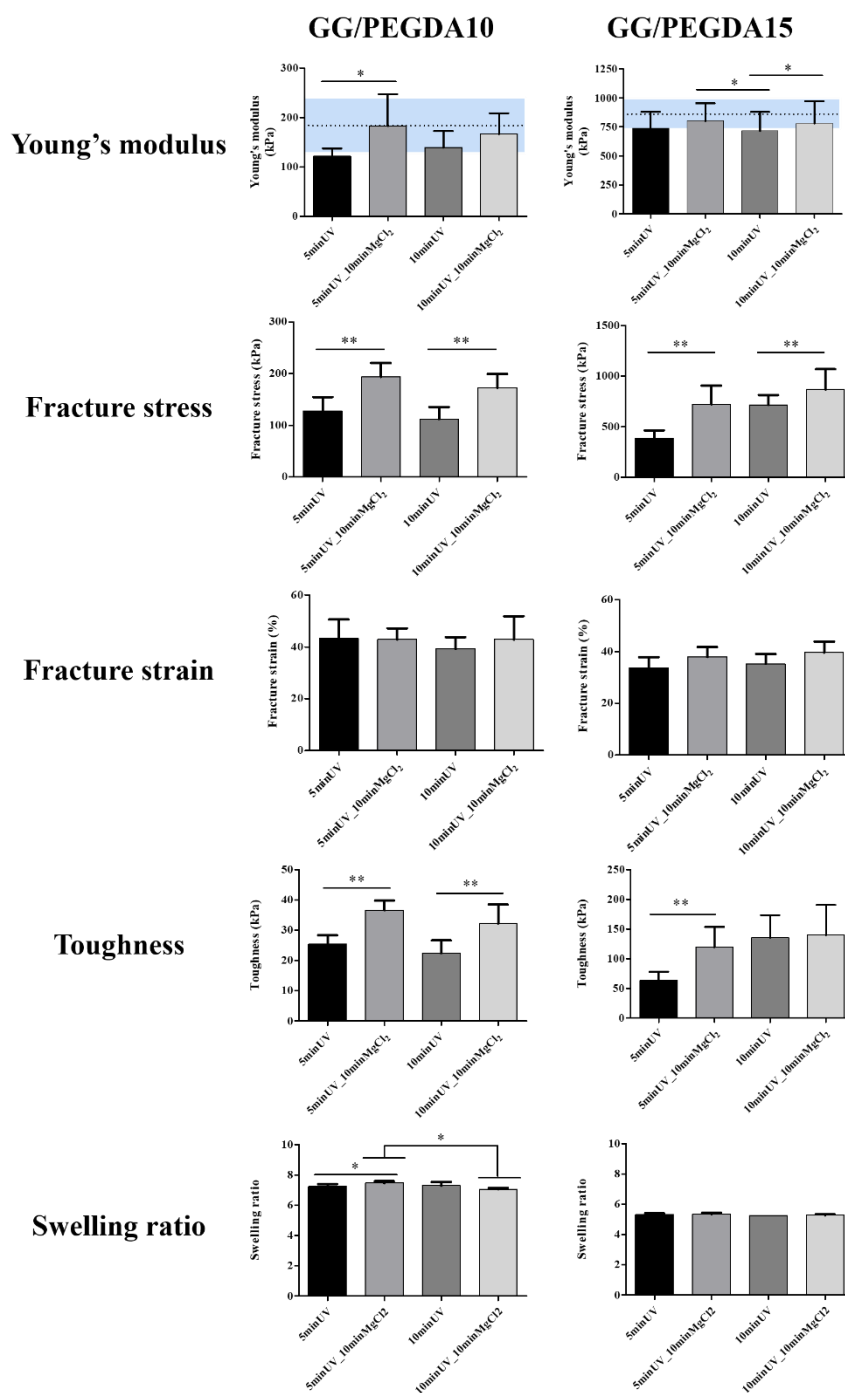


Figure 2. Mechanical characterization of GG/PEGDA10 and GG/PEGDA15 hydrogels, in terms of: Young's modulus, fracture stress, fracture strain, toughness and swelling ratio. For the Young's modulus, the blue areas represent the range of stiffness reported in O'Connell et al.^[6b] for the native articular cartilage. *p < 0.05, **p < 0.01, n = 5.

Analyzed samples: GG/PEGDA10_5minUV, GG/PEGDA10_5minUV_10minMgCl₂, GG/PEGDA10_10minUV, GG/PEGDA10_10minUV_10minMgCl₂, GG/PEGDA15_5minUV, GG/PEGDA15_5minUV_10minMgCl₂, GG/PEGDA15_10minUV, GG/PEGDA15_10minUV_10minMgCl₂.

1 The effects of UV exposure time and ionic crosslinking with MgCl_2 were analyzed for each
2
3 PEGDA concentration. The Young's modulus of GG/PEGDA10 hydrogels photo-crosslinked
4
5 for 5 min using a UV light source emitting at 365 nm at an intensity of 40 mW cm^{-2} , was
6
7 significantly improved by ionic crosslinking from an average value of $122 \pm 16 \text{ kPa}$ (without
8
9 ionic crosslinking, GG/PEGDA10_5minUV) to $182 \pm 65 \text{ kPa}$ (with ionic crosslinking
10
11 GG/PEGDA10_5minUV_10minMgCl₂) ($p < 0.05$). Differently, no statistical difference was
12
13 found between hydrogels photo-crosslinked for 10 min at the same conditions of wavelength
14
15 and intensity described above (without ionic crosslinking, GG/PEGDA10_10minUV), showing
16
17 a Young's modulus of $139 \pm 33 \text{ kPa}$, and hydrogels similar, but subjected to ionic crosslinking
18
19 (with ionic crosslinking GG/PEGDA10_10minUV_10minMgCl₂), resulting in a modulus of
20
21 $166 \pm 42 \text{ kPa}$. On the other hand, the Young's modulus of GG/PEGDA15 hydrogels photo-
22
23 crosslinked for 5 min (same conditions as before) improved from an average value of $738 \pm$
24
25 142 kPa (without ionic crosslinking, GG/PEGDA15_5minUV) to $801 \pm 152 \text{ kPa}$ (with ionic
26
27 crosslinking, GG/PEGDA15_5minUV_10minMgCl₂), but without any statistical difference.
28
29 Finally, increasing the time of photopolymerization to 10 minutes, a statistically significant
30
31 difference ($p < 0.05$) in the Young's modulus was found, between absence ($715 \pm 163 \text{ kPa}$,
32
33 GG/PEGDA15_10minUV) and presence ($780 \pm 190 \text{ kPa}$,
34
35 GG/PEGDA15_10minUV_10minMgCl₂) of ionic crosslinking.
36
37

38
39
40
41
42
43
44
45 These results, together with the ones shown in Figure S1, demonstrate that the PEGDA
46
47 concentration can modulate the rather low mechanical properties of GG, in agreement with
48
49 other reports.^[34] Indeed, the properties of PEGDA can be varied by acting on its molecular
50
51 weight, concentration, photo-initiator concentration and crosslinking parameters such as
52
53 exposure time.^[35] The scientific literature also confirms the relevant role of ionic-crosslinking
54
55 in the improvement of hydrogels Young's moduli.^[36] Only one study focused on analyzing the
56
57 blend of GG and PEGDA (Mn: 6000), even if its primary purpose was the evaluation of the
58
59
60
61
62
63
64
65

1 blend printability. In this study, 1.5 % GG blended with 10 % PEGDA was analyzed and a
2 comparison between the Young's moduli of this material in different conditions (non-
3 crosslinked, photo-crosslinked and, double (photo- and ionic) was made. The Young's modulus
4 evaluated through compression tests was improved from 40 kPa to 60 kPa and to 184 kPa,
5 respectively, for the above-mentioned crosslinking conditions.^[36] In our case, the combination
6 between GG and PEGDA and the possibility to increase the UV exposure time and PEGDA
7 concentration allowed achieving values closer to the ones featuring the different zones of the
8 human AC, namely 280 ± 160 kPa (superficial) and 730 ± 260 kPa (deep), evidenced with blue
9 regions in the graphs of Figure 2, which constitutes an original result, for this material.

10
11
12
13
14
15
16
17
18
19
20
21
22 The adoption of a dual crosslinking strategy (optical and chemical one) also allowed to
23 modulate other important mechanical features of the hydrogels. The fracture stress of
24 GG/PEGDA10 hydrogels photo-crosslinked for 5 min was significantly improved from $127 \pm$
25 27 kPa (without ionic crosslinking, GG/PEGDA10_5minUV) to 194 ± 27 kPa (with ionic
26 crosslinking, GG/PEGDA10_5minUV_10minMgCl₂) ($p < 0.01$). Similarly, the fracture stress
27 for hydrogels photo-crosslinked for 10 min was significantly improved from 112 ± 23 kPa
28 (GG/PEGDA10_10minUV) to 173 ± 26 kPa using the ionic crosslinking
29 (GG/PEGDA10_10minUV_10minMgCl₂) ($p < 0.01$). The same behavior was found in
30 GG/PEGDA15 hydrogels in which the ionic crosslinking significantly improved the fracture
31 stress of photo-crosslinked materials ($p < 0.01$). Interestingly, the fracture strain of both
32 GG/PEGDA10 and GG/PEGDA15 hydrogel formulations did not show any significant
33 difference between the groups, ranging from values slightly larger than 40 % for the hydrogels
34 mimicking the superficial cartilage and slightly smaller than 40 % for the hydrogels mimicking
35 the deep cartilage. Such values can be considered suitable for the application in the cartilage
36 TE field, being superior to the ones possessed by the native AC.^[5]

1
2
3
4
5
6
7
8
9
10
11
12
13
14
15
16
17
18
19
20
21
22
23
24
25
26
27
28
29
30
31
32
33
34
35
36
37
38
39
40
41
42
43
44
45
46
47
48
49
50
51
52
53
54
55
56
57
58
59
60
61
62
63
64
65

Moreover, the toughness of both GG/PEGDA10 and GG/PEGDA15 hydrogels resulted statistically different between samples treated with or without ionic crosslinking ($p < 0.01$). The toughness of GG/PEGDA10 was improved of around 1.5 fold when ionic crosslinking was applied for both photopolymerization times, whereas the toughness of GG/PEGDA15 hydrogels was improved significantly from 64 ± 14 kPa (GG/PEGDA15_5minUV) to 119 ± 34 kPa (GG/PEGDA15_5minUV_10minMgCl₂) (5 min of photopolymerization) ($p < 0.01$). The toughness values of GG/PEGDA15_10minUV and GG/PEGDA15_10minUV_10minMgCl₂ (10 min photopolymerization) were not significantly different, being 136 ± 34 kPa and 140 ± 50 kPa, respectively.

The hydrogel formulations described above showed interesting mechanical properties, which had not been deeply investigated, so far, in the state-of-the-art concerning this material type. Interestingly, the results highlighted that ionic crosslinking with MgCl₂ in addition to DMEM led to a statistically significant improvement of the Young's modulus, fracture stress and toughness. Besides, 5 min of UV exposure for each layer allowed keeping the crosslinking time lower while maintaining an optimal polymerization degree. The contribution of ionic crosslinking proved more effective than the UV exposure time. In fact, an overall increase in the mechanical properties of the hydrogels was observed, when comparing the samples crosslinked with the same UV light timing but with the additional ionic crosslinking with MgCl₂. This enhancement is probably due to an increase in the number of divalent cations (Mg²⁺) that promoted the aggregation of GG chains and formed a more robust polymer network structure. Among the candidate divalent cations, MgCl₂ was chosen because it proved to have a positive effect on cartilage tissues affected by degenerative diseases, like osteoarthritis.^[37]

Several blend compositions with various mechanical properties have been developed in the cartilage TE field, so far. Strontium alginate (Alg-Sr) and strontium alginate/chondroitin sulfate (Alg/CS-Sr) hydrogels have been proposed as interesting blends with tunable mechanical

1
2
3
4
5
6
7
8
9
10
11
12
13
14
15
16
17
18
19
20
21
22
23
24
25
26
27
28
29
30
31
32
33
properties for cartilage TE. Both blends showed intriguing biological features, but their
compression Young's moduli were far from the target values featuring the natural AC (less than
60 kPa for Alg-Sr and less than 120 kPa for Alg/CS-Sr).^[38] Another study focused on the
development of an interpenetrating hydrogel made of Agar and polyacrylamide (PAAm), which
were physically and ionically crosslinked. The resulting hydrogels exhibited a linear stiffness
that improved by increasing the Agar concentration up to 313 kPa (30 mg/mL), a value which
is far from the desired one (581 ± 168 kPa^[5, 6b, 7]), if full-thickness cartilage tissue substitution
is targeted.^[39] Fully synthetic hydrogels, composed of poly (2-acrylamido-2-
methylpropanesulfonic acid) (PAMPS) and poly (N-isopropylacrylamide-co-acrylamide)
[P(NIPAAm-co-AAm)], were also evaluated as potential off-the-shelf materials for cartilage
replacement.^[40] These hydrogels have been developed without reproducing cartilage-specific
zones and achieving 1 MPa as a target Young's modulus: this value could be too high for human
cartilage tissue substitution. Moreover, these hydrogels were hard to be developed *in situ* due
to reactions that typically produce toxic compounds.

34
35
36
37
38
39
40
41
42
43
44
45
46
47
48
49
50
51
52
53
54
55
56
57
In addition to the mechanical analyses, the swelling ratio of the different samples was calculated,
to get hints on the crosslinking density of each material formulation and to verify if there were
any significant changes due to different concentrations and/or different crosslinking parameters.
Figure 2 also shows that the different crosslinking parameters, while keeping the same PEGDA
concentration, did not significantly modify the swelling degree. On the other hand, different
PEGDA concentrations produced different swelling ratios. This indicates a higher crosslinking
density for GG/PEGDA15 hydrogels, as also confirmed by mechanical properties. Based on
the results obtained, we chose the best candidates (GG/PEGDA10_5minUV_10minMgCl₂ and
GG/PEGDA15_5minUV_10minMgCl₂), namely the ones showing mechanical properties as
close as possible to the ones of the superficial and deep zones of the AC.^[7b]

58 **2.2 Hydrogel doped with graphene oxide**

59
60
61
62
63
64
65

1 GO which is known for its remarkable mechanical and lubrication properties, was selected for
2 doping the GG/PEGDA10_5minUV_10minMgCl₂ hydrogel (the one mimicking the superficial
3 AC zone). Previous studies showed that GG is a suitable reducing agent for stabilizing the
4 dispersion of nanofillers in aqueous solutions.^[41] However, only a few studies have explored
5 the combination of GG and carbon-based dopants to improve the mechanical properties of these
6 hydrogels.^[42]

7
8
9
10
11
12
13
14 GO was synthesized using the modified Hummer's method.^[43] Figure 3a and Figure 3b show
15 SEM images and Raman spectrum (with a laser wavelength of 532 nm) of the layered GO bulk.
16 Raman analysis confirmed the two characteristic bands at 1360 cm⁻¹ (D band) and 1606 cm⁻¹
17 (G band) related to GO. After sonication of the GO in ethanol, a droplet from the dispersion
18 was dropcasted on a Si/SiO₂ wafer and let dry overnight; this allowed to observe flakes with a
19 minimum average thickness of 4.0 ± 0.3 nm which was measured using atomic force
20 microscopy (AFM; Figure 3c). Additionally, we performed high-resolution transmission
21 electron microscopy (HRTEM) to confirm the layered structure of GO at the nanoscale (Figure
22 3d).
23
24
25
26
27
28
29
30
31
32
33
34
35
36
37
38
39
40
41
42
43
44
45
46
47
48
49
50
51
52
53
54
55
56
57
58
59
60
61
62
63
64
65

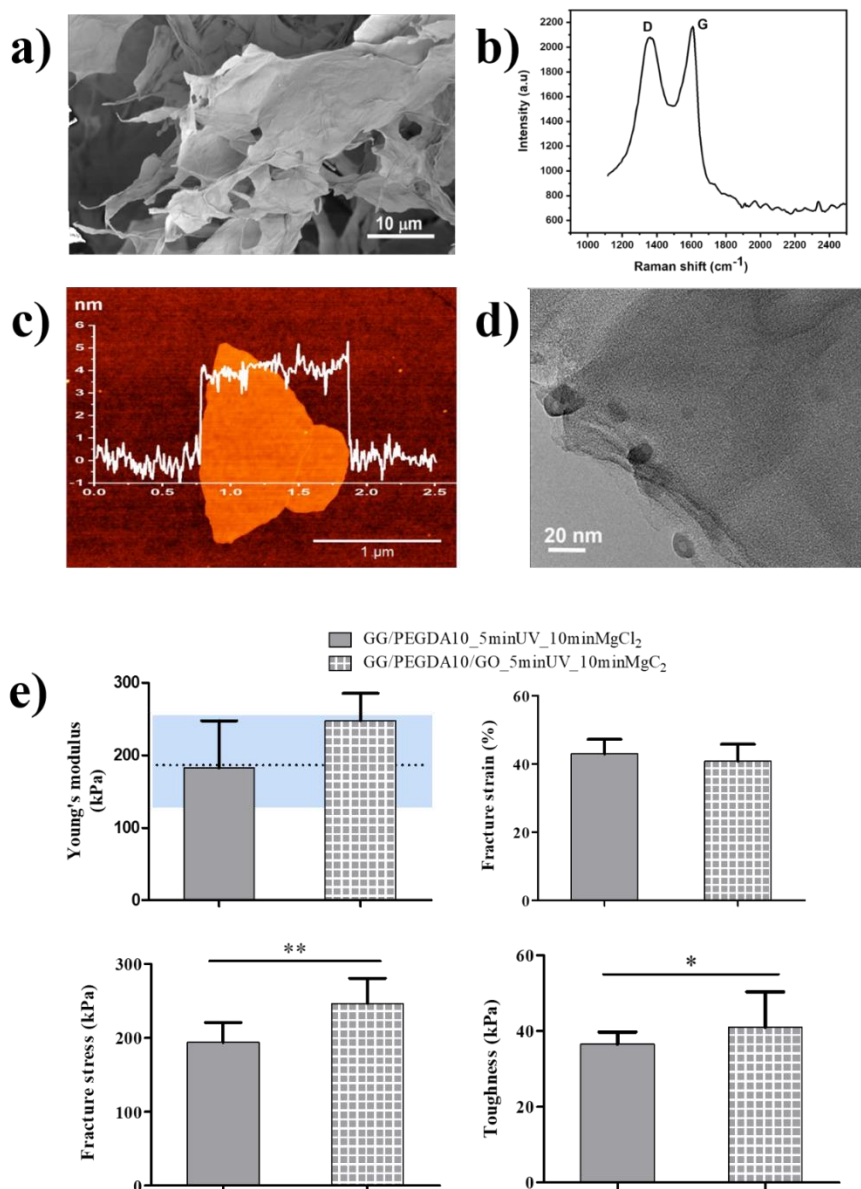


Figure 3. Characterization of GO and its inclusion in the hydrogel: a) SEM images of layered GO flakes; b) Raman spectrum at 532 nm; c) AFM measurements of a dispersed GO demonstrated minimal thickness of 4.0 ± 0.3 nm ($n = 5$); d) HRTEM image, confirming the layered structure of a dispersed GO. e) Analysis of the nanocomposite GG/PEGDA10/GO_5minUV_10minMgCl₂: Young's modulus, fracture stress, fracture strain and toughness. For the Young's modulus, the blue areas represent the range of stiffness featuring the superficial articular cartilage, reported in).^[6b] * $p < 0.05$, ** $p < 0.01$, $n = 5$.

Analyzed samples: GG/PEGDA10_5minUV_10minMgCl₂, GG/PEGDA10/GO_5minUV_10minMgCl₂.

GO (0.01 % w/v) was added, as mentioned, to the GG/PEGDA10_5minUV_10minMgCl₂ hydrogel formulation, obtaining a homogeneous dispersion of the nanomaterial in the matrix (Figure S2). This was facilitated by the low concentration used (0.01 % w/v), which also

1 minimizes the cytotoxicity risk of GO, which is known to be dose-dependent.^[44] With the
2 concentration used in this paper, previous reports highlighted an increased mesenchymal stem
3 cell (MSCs) growth with respect to the controls, thus resulting beneficial, rather than toxic.^[45]
4
5 The mechanical properties of GG/PEGDA10_5minUV_10minMgCl₂ and the corresponding
6
7 GO-doped hydrogel (GG/PEGDA10/GO_5minUV_10minMgCl₂) were compared in order to
8
9 assess the role of GO in modulating the behavior of samples photo-crosslinked for 5 min and
10
11 subsequently ionically crosslinked with MgCl₂ (Figure 3e). The use of such a concentration of
12
13 GO led to a slight increase (not statistically significant) in the hydrogel stiffness (from $182 \pm$
14
15 26 kPa to 248 ± 21 kPa). However, the stiffness of the nanocomposite was still included in the
16
17 range featuring the native human superficial cartilage zone.^[6b] The fracture strain did not
18
19 change with the addition of the nanofiller. On the other hand, the average value of fracture
20
21 stress and toughness increased significantly, from 194 ± 27 to 246 ± 34 kPa and from 36 ± 3 to
22
23 41 ± 9 kPa, respectively. The toughness of the GO-doped hydrogel showed an improvement,
24
25 probably due to the higher energy dissipation in the presence of GO nanosheets, highlighting a
26
27 better mechanical performance than the bare hydrogel. ^[46] As well, fracture stress increased
28
29 thanks to the dopant agent, which acted as a reinforcement agent of synthetic cartilage tissue.
30
31 These results are in line with other pieces of evidence available in the scientific literature.^[47]
32
33 For example, in poly (vinyl alcohol) (PVA)/GO nanocomposite hydrogels, a significant
34
35 reinforcement was ascribed to the formation of a dense and stable crosslinking network at
36
37 different concentrations of the polymer due to the presence of micron-sized GO (~ 0.3 % w/v).
38
39 In our case, the introduction of a relatively low concentration of GO (0.01 % w/v) did not lead
40
41 to a statistical difference with the bare hydrogel in term of Young's modulus, thus allowing to
42
43 remain in the range of the target value for mimicking the superficial AC tissue. Nevertheless,
44
45 other crucial mechanical properties, such as fracture stress and toughness, were significantly
46
47 improved, thus highlighting that even a low concentration of GO can guarantee important
48
49
50
51
52
53
54
55
56
57
58
59
60
61
62
63
64
65

reinforcing mechanisms.^[48] Moreover, we observed that the swelling ratio slightly decreased by adding the GO nanofiller (from 7.2 ± 0.2 to 6.5 ± 0.3), but without any statistical significance. Lubrication tests were performed on the superficial cartilage-mimicking samples (GG/PEGDA10_5minUV_10minMgCl₂ and GG/PEGDA10/GO_5minUV_10minMgCl₂) in order to assess if the presence of the GO nanosheets could improve lubrication properties. A depiction of the set-up for the evaluation of the lubrication properties is shown in Figure 4a. The lubrication test was divided into three intervals, according to the Stribeck curve, which provides information on the different friction regimes.^[49] In the first interval, the system was allowed to relax before the next applied load; in the second interval, the rotational speed (10 min⁻¹) and normal force (0.5 N) were increased (up-curve); finally, the rotational speed was decreased (down-curve). This analysis allowed analyzing the evolution of friction in the static regime and the transition from the static to the kinetic one.

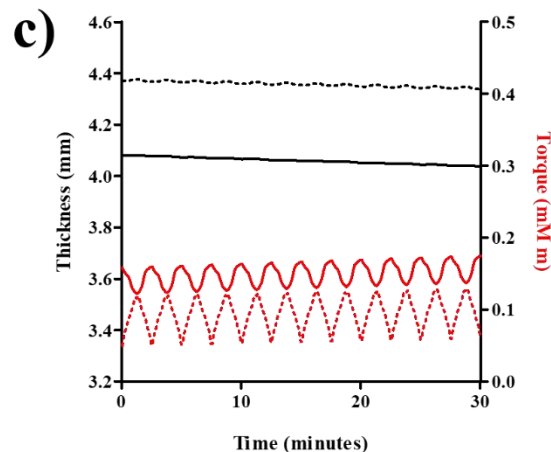
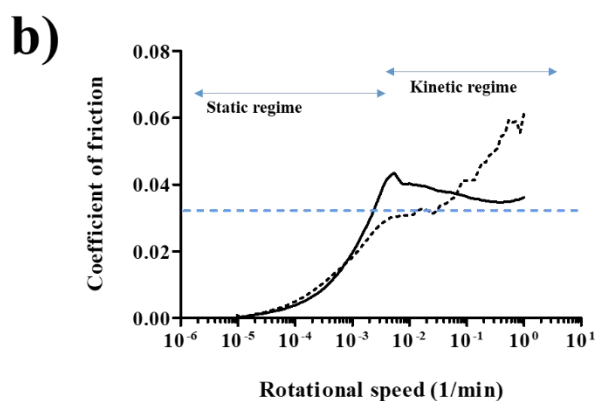
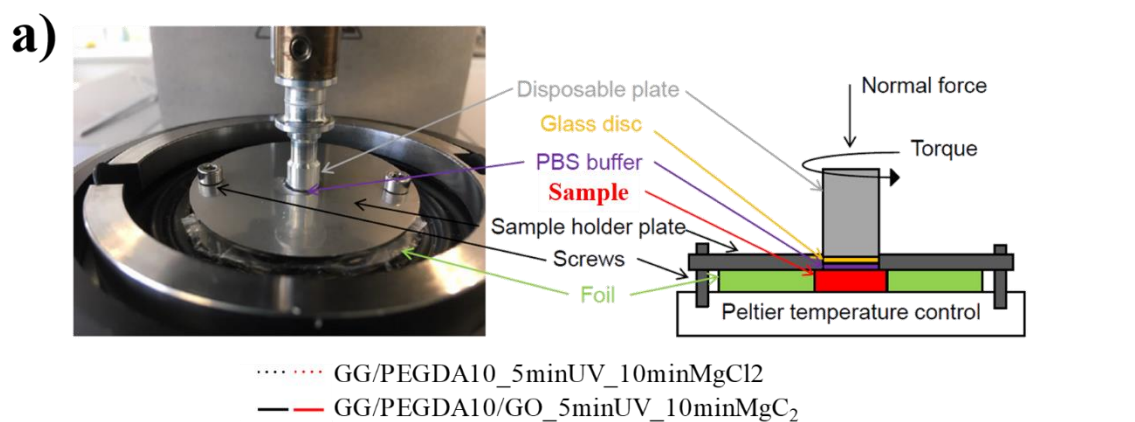


Figure 4. a) Depiction of the set-up used for testing of hydrogels (red block). b) Lubrication analysis of the composite hydrogels according to the Stribeck curve: the transition from static to dynamic friction is marked with arrows in the diagram. The blue line represents the coefficient of friction of the articular cartilage. c) Analysis of the wear and the torque applied on the hydrogel through the rheometer. Analyzed samples: GG/PEGDA10_5minUV_10minMgCl₂, GG/PEGDA10/GO_5minUV_10minMgCl₂

As shown in Figure 4b, the coefficient of friction (COF) gradually grew in the static regime for both GG/PEGDA10_5minUV_10minMgCl₂ and GG/PEGDA10/GO_5minUV_10minMgCl₂ hydrogels and a slightly higher value was observed for the doped sample. Nonetheless, for higher rotational speeds, in the kinetic regime, the COF of GG/PEGDA10/GO_5minUV_10minMgCl₂ stabilized, whereas the COF of GG/PEGDA10_5minUV_10minMgCl₂ maintained an increasing trend, reaching significantly higher values. The lubrication provided by the doped formulation was thus effective in stopping the increment of the COF. Moreover, it slightly decreased with rotational speed. Results demonstrate that the non-doped formulation possesses a slightly smaller COF in the static regime than the doped one, compatible with the range found for the AC, while the GO nanofiller dispersed into the hydrogel was able to markedly improve the lubrication properties of the bare formulation in the kinetic regime.

The tribological properties of graphene mainly depend on its structure.^[50] GO might exhibit a slightly larger COF than graphene caused by the presence of exposed interlayer hydrogen bonds, even if it confers a longer lifetime and wear life because it promotes layer slipping mechanisms. This is extremely important for bear-wearing applications, as in the field of materials for cartilage substitution. As demonstrated by Tang et al.^[51], GO with a relatively large lateral size (in our case, approximately 4 μm) guarantees lubricity by the sliding along the basal plane of its crystalline lamellar structure. The authors also analyzed the lubricant behavior of increasing concentrations of GO (from 0.05 % to 1.5 % w/v) in a water-based lubricant solution, claiming that there is a sort of threshold (in their case 0.1 % w/v) above which GO, similarly to other nanomaterials, can decrease its lubricant effect.^[52] The concentration of GO adopted in this

1 work (0.01 % w/v) is well below such a threshold value. Also, Meng et al.^[47b], investigated
2 different concentrations of GO embedded into PVA nanocomposite hydrogels lubricated with
3
4 FBS (up to 2 % w/v). Their results showed that the minimum COF (close to 0.07) was found
5
6 for the GO concentration of 1.5 % w/v, while it resulted higher for all the other concentrations
7
8 tested (above and below 1.5 % w/v). It is important to underline that the lubrication properties
9
10 achieved by these authors were inferior to the results reported in this work. Furthermore, the
11
12 use of such a high concentration of GO (1.5 % w/v) could severely influence cell viability due
13
14 to cytotoxic effects.
15
16

17
18
19 Figure 4c shows the results of a wear test performed through a rheometer: it can be observed
20
21 that for both samples, GG/PEGDA10_5minUV_10minMgCl₂ and
22
23 GG/PEGDA10/GO_5minUV_10minMgCl₂, the thickness of the hydrogel remained relatively
24
25 constant during the whole test, as well as the applied torque. The oscillation was probably due
26
27 to the elastic deformation of the hydrogel specimen. Native AC possesses considerable
28
29 lubricant properties in order to withstand the cyclical stresses due to the daily life activities of
30
31 people. The addition of GO was demonstrated to be effective in keeping the COF at a value
32
33 close to the native AC one (0.03).^[6b] Furthermore, the doped formulation did not show any
34
35 preliminary signs of wear. Lubricity and wear represent crucial factors for many biomedical
36
37 applications, especially those related to cartilage tissue substitution.^[53]
38
39
40
41
42

43 **2.3 Full cartilage-mimicking bilayered hydrogel**

44
45 Figure 5a shows the fabrication procedure of bilayered hydrogels by sequentially adding each
46
47 specific hydrogel formulation in a polydimethylsiloxane (PDMS) mold. The model described
48
49 in the following permitted, by using the mechanical data reported in section 3.1, to find
50
51 appropriate volumetric proportions for building a bilayered hydrogel structure, whose overall
52
53 properties could be similar to the ones of a healthy human AC (a full-thickness tissue, including
54
55 all the different zones described in the Introduction section). It has been assumed that the
56
57 composite material was isotropic and composed of two zones (deep and superficial), which
58
59
60
61
62
63
64
65

contribute to the final stiffness of the composite material in direct proportion to their volume fraction.^[54] The volumetric fraction of deep cartilage (f_{DC}) and superficial cartilage (f_{SC}) for cylindrical hydrogels is the ratio between the deep or superficial cartilage volume and the total volume, described as:

$$f_{DC} = \frac{V_{DC}}{V_{tot}} = \frac{\pi r^2 h_{DC}}{\pi r^2 h_{tot}} = \frac{h_{DC}}{h_{tot}} \quad (1)$$

$$f_{SC} = \frac{V_{SC}}{V_{tot}} = \frac{\pi r^2 h_{SC}}{\pi r^2 h_{tot}} = \frac{h_{SC}}{h_{tot}} \quad (2)$$

where r is the radius of the crosslinked hydrogel disc, h_{DC} , h_{SC} and, h_{tot} are the heights of deep cartilage, superficial cartilage and the total disc (deep + superficial), respectively. Moreover, the relationship between deep and superficial volumetric fractions is:

$$f_{DC} + f_{SC} = 1 \quad (3)$$

The equivalent Young's modulus of the bilayered structure can be expressed by applying the Reuss model as follows:

$$E_{cartilage} = \frac{E_{DC} E_{SC}}{f_{SC} E_{DC} + f_{DC} E_{SC}} \quad (4)$$

where $E_{cartilage}$, E_{DC} and, E_{SC} are the Young's modulus of the healthy cartilage, the one of the deep cartilage hydrogel, and the one of the superficial hydrogel, respectively.

Substituting the relationship (3) in (4), f_{deep} can be obtained as:

$$f_{DC} = \frac{E_{DC} E_{SC}}{E_{cartilage} - E_{SC}} * \frac{1}{E_{SC} - E_{DC}} \quad (5)$$

Subsequently, f_{DC} was substituted in (1) to find h_{DC} as:

$$h_{DC} = f_{DC} h_{tot} \quad (6)$$

Finally, the expression (6) was substituted into the definition of h_{tot} to calculate h_{SC} as:

$$h_{SC} = h_{tot} - h_{DC} \quad (7).$$

Fixed any height, to calculate the volumetric fractions of deep and superficial layers, E_{DC} and E_{SC} were considered equal to 864 kPa and 182 kPa, respectively (data derived from the

mechanical characterization of hydrogels), while $E_{cartilage}$ was considered equal to 500 kPa, based on literature data.^[6b, 55]

Using the model, we obtained the volumetric fraction of the superficial (GG/PEGDA10/GO_5minUV_10minMgCl₂) and deep (GG/PEGDA15_5minUV_10minMgCl₂) layers equal to 19.43% and 80.57%, respectively. This analysis partially reflects the real situation of native AC, in which the superficial layer constitutes the 10-20% of the overall cartilage thickness.^[56]

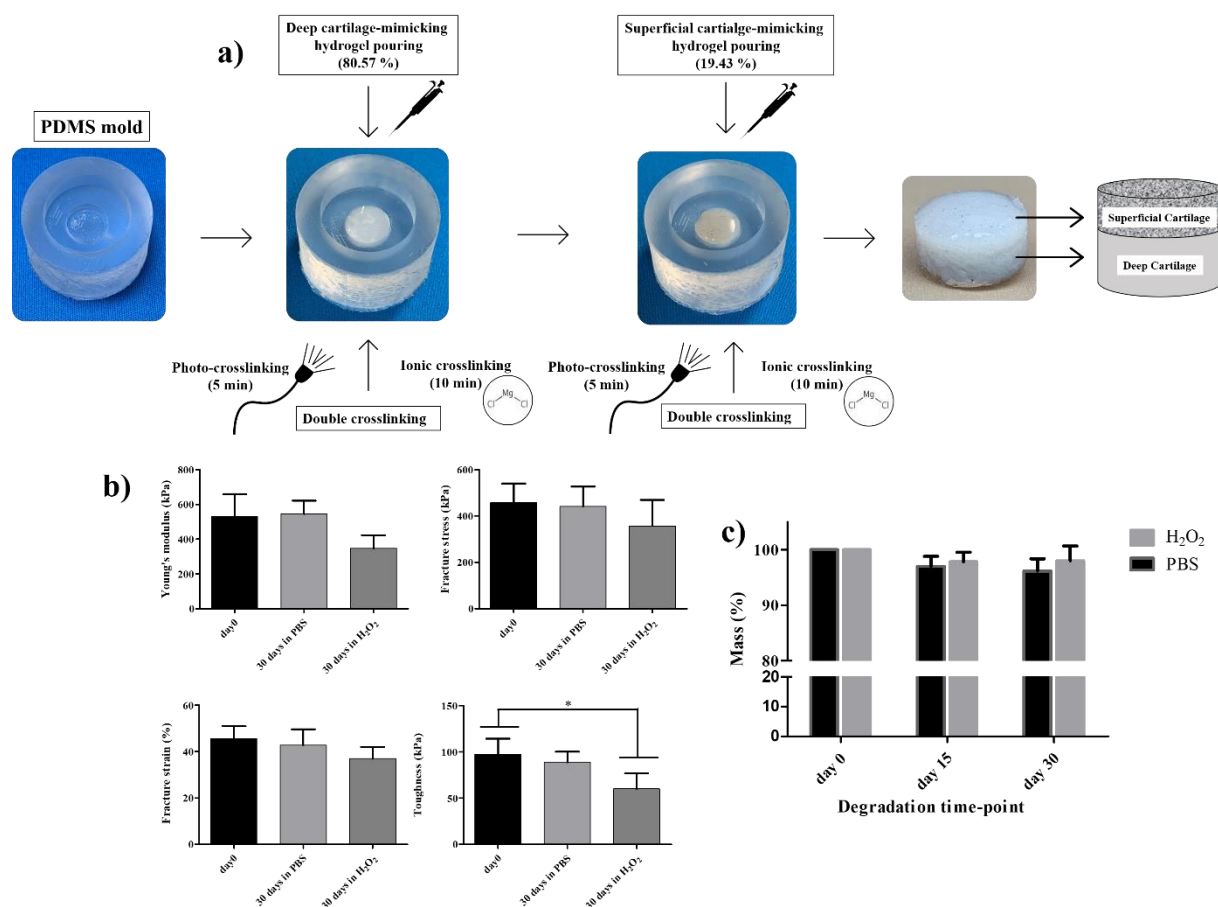


Figure 5. (a) Depiction of the sequential fabrication procedure used to assemble the cylindrical bilayered hydrogels into PDMS molds. b) Mechanical analysis of the bilayered hydrogels after 30 days incubation in PBS and H₂O₂ in terms of: Young's modulus, fracture stress, fracture strain and toughness. c) Analysis of the total mass variation overtime, upon incubation in PBS and H₂O₂, * $p < 0.05$, $n = 4$.

In the state-of-the-art, similar models were developed for predicting composite hydrogel moduli, once given the mechanical properties of the different constitutive materials. Previous studies

1 reported the use of a model to calculate the volumetric fraction of sol-gel composites.^[57]

2 Isostress within isostrain models were used to describe the mechanical behaviors of poly(2-
3 acrylamido-2-methylpropanesulfonic sodium) (PNaAMPS) dispersed into neutral
4 polyacrylamide (PAAm) hydrogels at small deformation.^[57c] Moreover, an isostress model was
5 developed and validated to predict the mechanical responses of cellulose nanocrystals (CNC)-
6 reinforced poly(2-hydroxyethyl methacrylate) (PHEMA) nanocomposite hydrogels.^[57a]
7 However, no multilayered structures using different materials or different concentrations of
8 blended materials have been modeled to predict their whole elastic modulus, in the field of
9 cartilage substitution.
10

11 Once fabricated, the mechanical characterization of the bilayer was performed to compare the
12 consistency of the model results with the experimental ones, also evaluating the stability of the
13 hydrogel after incubation in physiological medium (PBS) or inflammatory-like conditions
14 (H_2O_2) up to 30 days. Interestingly, the average Young's modulus of the bilayer (529 ± 128
15 kPa) was very close to the value of the healthy AC (500 kPa), used to apply the model. As
16 shown in Figure 5c, the Young's modulus, fracture stress, fracture strain and toughness did not
17 vary after one month in PBS. Slightly more evident differences were found after incubation in
18 H_2O_2 , especially regarding toughness. H_2O_2 accounts for a more aggressive condition, used to
19 predict long- term oxidative degradation through a short- term test. Indeed, induced oxidative
20 stresses can affect both GG and PEGDA.^[58] However, even the most affected parameter,
21 namely the toughness, remained close to the one owned by the native AC, namely about 47
22 kPa^[59], also in the worst case. These results demonstrate that one month of incubation produced
23 no marked mass loss in the tested samples, even if there was a slight effect on the material
24 mechanical properties, induced by the oxidative stresses of H_2O_2 . Probably, a change of the
25 polymer chain interactions might occur during the continuous presence of an inflammatory
26 condition.
27
28
29
30
31
32
33
34
35
36
37
38
39
40
41
42
43
44
45
46
47
48
49
50
51
52
53
54
55
56
57
58
59
60
61
62
63
64
65

2.4 Wear test

1
2 To perform a wear test, the bilayered hydrogels described in the previous section were
3
4 fabricated within a menisci-like phantom, as described in Figure 6a.
5
6

7 The wear test was performed using a four-station displacement control knee joint simulator
8
9 under fetal bovine calf serum-based solution that mimics the knee synovial fluid. A vertical
10
11 load was applied and the test run with a frequency of 1.1 Hz.^[60] The applied load at a frequency
12
13 of 1.1 Hz described a full walk step that was simultaneously composed of 4 different knee
14
15 movements (trends), namely axial force, flexion-extension angle, intra-extra tibial rotation, and
16
17 front-rear motion. Figure 6b reports a general description of the system components and some
18
19 sequential pictures of the system while performing the test. A movie of the knee simulator
20
21 during the wear test is reported as Movie S1.
22
23
24
25
26
27
28
29
30
31
32
33
34
35
36
37
38
39
40
41
42
43
44
45
46
47
48
49
50
51
52
53
54
55
56
57
58
59
60
61
62
63
64
65

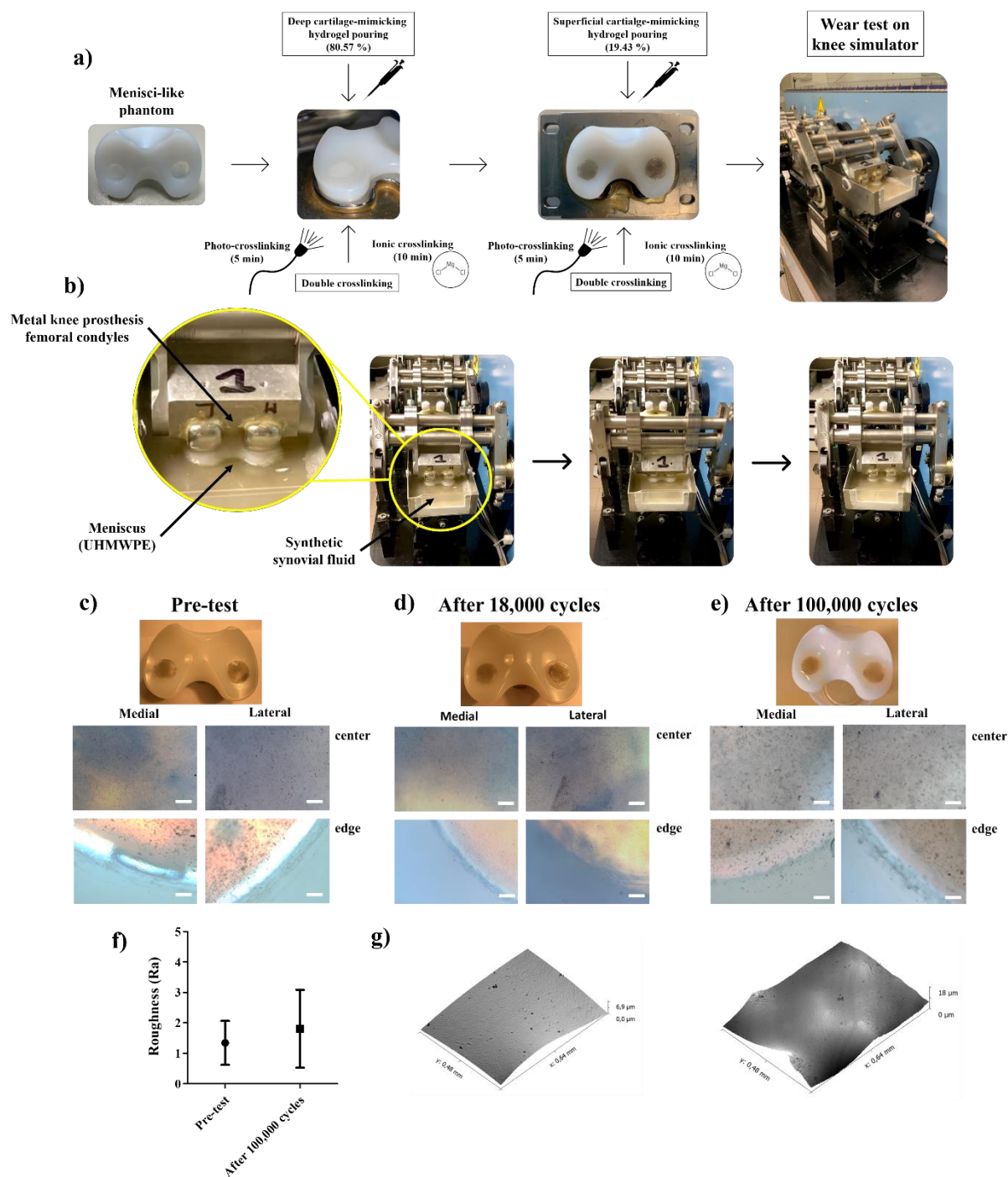


Figure 6. (a) Depiction of hydrogels fabrication within a menisci-like phantom. b) Depiction of the knee simulator set-up. Sequential images of the knee simulator movements during the wear test (see also Movie S1). In the zoomed image, it is possible to observe that the meniscus is immersed into fetal bovine calf serum-based solution and loaded by femoral condyles of metal knee prosthesis. c) Macroscopic and brightfield (4x) images of samples before wear test. d) Macroscopic and brightfield (4x) images of samples after 18,000 cycles. e) Macroscopic and brightfield (4x) images of samples after 100,000 cycles. The brightfield images of medial and lateral condyles were captured in the center and on the edge of samples using an optical microscope. Scale bar: 250 μm . f) Roughness measurements using optical profilometer of pre-tested and tested (100,000 cycles) bilayered hydrogels. g) Surface images captured using optical profilometer of pre-tested (left) and tested (right) bilayered hydrogels. $n = 4$.

1 Macroscopic visual examination of all knee-retrieved components revealed a consistent wear
2 pattern between two subsequently ISO 14243 standard wear tests, as shown in Figure 6c-e.
3

4 A similar behavior was observed between the medial and the lateral condyles of the specimens.
5

6 After 18,000 cycles, we observed that both condyles remained perfectly intact (Figure 5d) both
7 in the center and at the edges, as the pre-test samples (Figure 6c). After 100,000 cycles on the
8 UHMWPE holes, we observed that the medial condyle showed some slight signs of wear
9 without delamination, while the lateral condyle remained intact (Figure 6e). We can suppose
10 that medial condyle hydrogel samples were subjected to delamination due to rubbing with the
11 prosthesis because the body load is transmitted through the menisci in different proportions
12 (70% in the lateral compartment and 50% in the medial compartment).^[61] Moreover, this effect
13 can be also partially due to a scarce adhesion between the UHMWPE hole and the hydrogel,
14 being the PE hydrophobic. No statistical differences were found in terms of roughness between
15 100,000 cycles-tested and pre-tested samples (Figure 6f), while slight signs of wear were
16 observed on the surface of the stressed hydrogel (Figure 6g). Despite the presence in the state-
17 of-the-art of different examples of cartilage-substituting hydrogels, to our knowledge, our study
18 is the first one assessing the functional behavior of the produced hydrogels by using this wear
19 test, adhering to the ISO 14243 standard. Thus, these results shed light on the cyclical resistance
20 of the fabricated hydrogels, which is of crucial importance for assessing their possible success
21 as an osteoarticular tissue substitute, but also highlight the need, in general, for an extensive
22 assessment of the wear behavior of hydrogels, in the state-of-the-art of this research field.
23

24 The test was conducted by combining all different walk movements following the ISO 14243
25 standard for 100,000 cycles that corresponded to evaluate standard human continuous walk for
26 around 24 h. Comparing these results with the ones obtained in a study in which natural
27 cartilage was tested, it is worth highlighting that already at 50,000 cycles, the cartilage tissue
28 undergoes damage, if continuously solicited.^[62] We can thus claim that the fabricated bilayer
29
30
31
32
33
34
35
36
37
38
39
40
41
42
43
44
45
46
47
48
49
50
51
52
53
54
55
56
57
58
59
60
61
62
63
64
65

1 showed an excellent behavior when subjected to a high number of cycles and can thus be
2 considered a suitable functional cartilage substitute.
3

4 It is important to underline that the materials described in this study could be injected directly
5 in chondral defects through syringes-like devices and sequentially crosslinked in situ.^[63] Indeed,
6 we preliminarily evaluated the printability of both hydrogel formulations mimicking the deep
7 and the superficial cartilage zones, finding encouraging results (Figure S3, Movie S2). However,
8 the potential application of such a bilayered hydrogel does not exclude the fabrication of the
9 construct outside the body and its subsequent surgical implantation (*e.g.*, through arthroscopic
10 procedures). Along this line, the use of computed tomography (CT) data would help in
11 obtaining the exact shape of chondral defects and then to fabricate defect-specific tissue
12 substitutes using customized molds.^[64]
13
14
15
16
17
18
19
20
21
22
23
24
25

26 **2.5 Cytotoxicity evaluation**

27 Finally, to evaluate the cytotoxicity of the superficial and deep hydrogels
28 (GG/PEGDA10/GO_5minUV_10minMgCl₂ and GG/PEGDA15_5minUV_10minMgCl₂), we
29 assessed viability and metabolic activity of human chondrocytes put in contact with the
30 supernatant collected from both hydrogels incubated in culture medium for 24 hours. Cell
31 viability and cell metabolic activity were checked after two and six days. Cell viability assessed
32 by Live and Dead (L/D) assay showed the presence of only viable cells (green stained), almost
33 without dead cells (red stained) at the analyzed time points in both experimental groups,
34 indicating that the hydrogel formulations did not affect cell viability (Figure 7a). The behavior
35 was similar among the cells put in contact with the hydrogels-derived media and the cells
36 cultured as a control group (chondrocyte simply grown in standard culture medium).
37
38
39
40
41
42
43
44
45
46
47
48
49
50
51
52

53 Furthermore, metabolic cell activity, evaluated by MTT assay, showed no statistical difference
54 at the two time points between the control and the experimental groups (Figure 7b). After six
55 days, the absorbance values were all lower than the ones found after two days. This result was
56
57
58
59
60
61
62

due to cell confluence after a week in culture, that determined a reduced metabolic activity in all samples analyzed, without any difference between control and experimental groups.^[65]

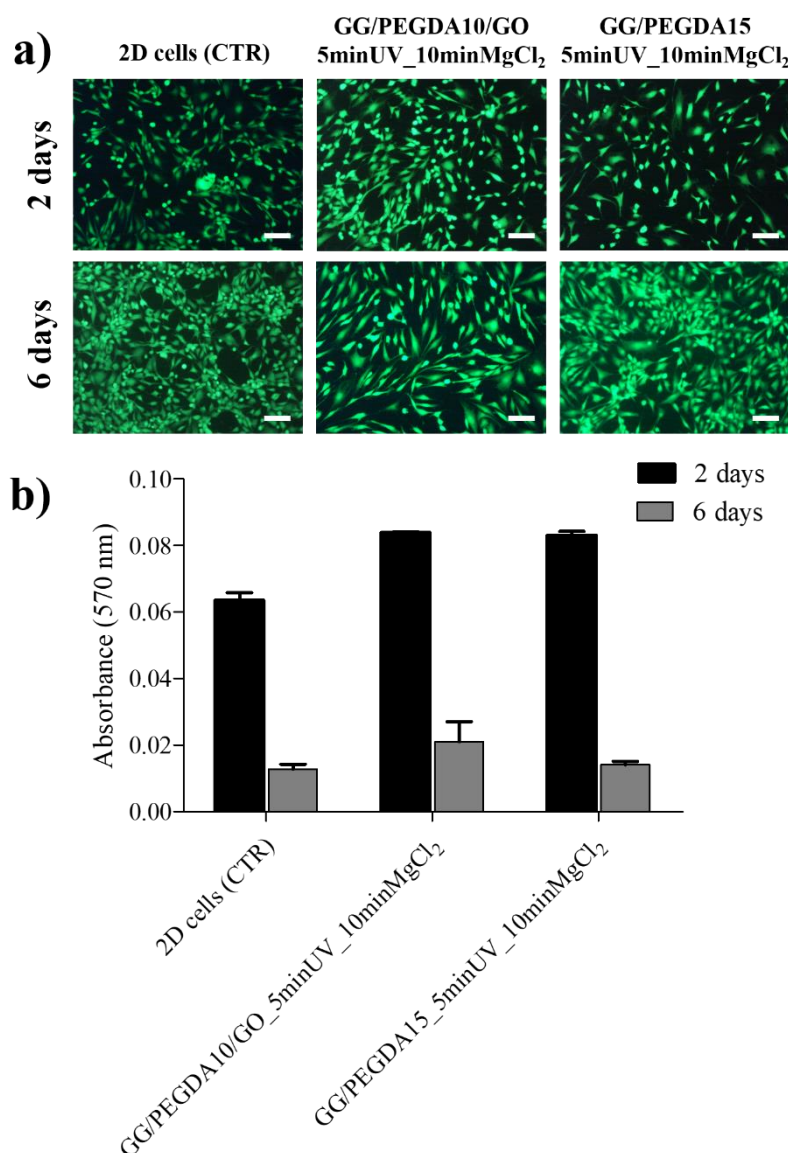


Figure 7. Live/Dead images of 2D chondrocytes untreated (CTR), treated with GG/PEGDA10/GO_5minUV_10minMgCl₂ supernatant, and treated with GG/PEGDA15_5minUV_10minMgCl₂ supernatant evaluated after 2 and 6 days. Viable cells are shown in green dead/necrotic cells are shown in red. Scale bars: 200 μ m. b) MTT test of the same samples evaluated after 2 and 6 days. n = 4.

Analyzed samples: GG/PEGDA10/GO_5minUV_10minMgCl₂, GG/PEGDA15_5minUV_10minMgCl₂

Cytocompatibility is a fundamental standard evaluation of cell viability for cartilage repair. Our data confirmed that the hydrogels did not affect this important parameter. Only three papers focused on different combinations of GG/PEGDA^[36, 66] and GG/GO^[67], but cell viability was

1
2
3
4
5
6
7
8
9
10
11
12
13
14
15
16
17
18
19
20
21
22
23
24
25
26
27
28
29
30
31
32
33
34
35
36
37
38
39
40
41
42
43
44
45
46
47
48
49
50
51
52
53
54
55
56
57
58
59
60
61
62
63
64
65

evaluated only in GG/PEGDA hydrogels. In line with our data, they have demonstrated that mesenchymal stromal cells embedded in GG/PEGDA showed a high percentage (above 87%) of viable cells.^[36] By contrast, other authors have shown that a different GG/PEGDA hydrogel formulation provided a unfavorable environment for mesenchymal stromal cells proliferation associated to an increase of cell apoptosis starting from third day.^[66]

3. Conclusion

We described the development of a bilayered hydrogel able to mimic the mechanical features of native AC and featured by enhanced lubrication properties. The bilayer was based on a combination of GG and PEGDA, and on two combined crosslinking approaches (physical and ionic). The resulting material proved to effectively modulate the mechanical properties of the superficial and the deep components of the bilayer. In this process, the influence of the ionic crosslinking was more relevant than the photo-crosslinking one. Two formulations were identified as the optimal ones to mimic the superficial and deep zones of the human articular cartilage.

GO nanosheets were synthesized in order to improve the lubrication properties of the top layer, thus to mimic the articular cartilage also in terms of low friction. Tribological analyses confirmed the beneficial effect of the addition of GO nanosheets into the top layer, in the kinetic regime. The nanocomposite also guaranteed improved mechanical properties, especially toughness.

By applying the Reuss model, we developed a bilayer structure mimicking the overall mechanical properties of the healthy articular cartilage, using two layers made of different hydrogel formulations and featured by specific thicknesses, which resulted as the output of the model. No cytotoxic effects were found on human chondrocytes up to 6 days, demonstrating the safety of the bilayered hydrogel. Moreover, a wear test confirmed that the bilayered construct can withstand physiologically relevant stresses up to 100,000 cycles. In conclusion,

1 the proposed biomimetic bilayered hydrogel is a promising candidate as a possible synthetic
2 substitute to be delivered into chondral and osteo-chondral defects in a minimally invasive way
3
4 and to restore the functional properties of the cartilage. Future *in vivo* tests will demonstrate the
5
6 pre-clinical and clinical suitability of such a composite material.
7
8
9

10 11 **4. Experimental Section**

12 ***Materials:***

13
14 Gellan gum (GG) powder (Gelzan[®], Merck) and poly (ethylene glycol) diacrylate (PEGDA,
15
16 Mn: 575, Merck) solution was used for the preparation of hydrogels. 2-hydroxy-4'-(2-
17
18 hydroxyethoxy)-2-methylpropiophenone (Irgacure 2959, I2959, Merck) was used as photo-
19
20 initiator, stocked in a mother solution made of dimethyl sulfoxide (DMSO, Merck). Magnesium
21
22 chloride hexahydrate (MgCl₂·6H₂O, Merck) diluted in deionized water was used to perform the
23
24 ionic crosslinking of hydrogels. Graphite flakes (99%, Alfa Aesar), H₂SO₄ (98%, Merck),
25
26 H₃PO₄ (98%, Merck), KMnO₄ (99%, Merck) and H₂O₂ (30% Merck) were used to synthesize
27
28 graphene oxide (GO) sheets. Wear tests were conducted using sodium azide (NaN₃, Merck) and
29
30 ethylenediaminetetraacetic acid (EDTA, Merck). Cell culture studies were conducted using low
31
32 glucose Dulbecco's Modified Eagle Medium (DMEM, Merck), fetal bovine serum (EuroClone),
33
34 penicillin/streptomycin (Gibco) and trypsin/EDTA (EuroClone, Merck). Cell viability studies
35
36 performed using phosphate buffered saline (PBS, Gibco) solution, Live/Dead[®]
37
38 Viability/Cytotoxicity Kit (Invitrogen) and metabolic activity by 3-(4,5-Dimethyl-2-thiazolyl)-
39
40 2,5-diphenyl-2H-tetrazolium bromide (MTT, Merck).
41
42
43
44
45
46
47
48
49

50 ***Preparation of superficial and deep cartilage hydrogels:***

51
52 Briefly, GG (1.75 and 1.67 % w/v) was dissolved in deionized water by magnetic stirring at
53
54 65°C for 1 h. After dissolution, the solutions were formed by adding PEGDA at a concentration
55
56 of 15% and 10% w/v, respectively. Both solutions were kept at 75 °C and agitated by magnetic
57
58 stirring for 1 h. Then, I2959 photo-initiator (0.1% w/v) was added in both solutions by
59
60
61
62
63
64
65

maintaining both temperature control and magnetic stirring active. Finally, each formulation was poured into cylindrical holes (diameter: 6 mm; height: 5 mm) of a custom-made PDMS mold. The photo-crosslinking was performed by UV light exposure using a UV optic fiber ($\lambda=365$ nm, Lightning cure LC5, Hamamatsu Photonics UK, Ltd) at an intensity of 40 mW cm^{-2} for 5 and 10 minutes. Some hydrogels underwent a further ionic crosslinking step through a first immersion into a MgCl_2 solution (1 % w/v in deionized water) for 10 minutes at room temperature (RO). Then, all the sample was finalized by incubation in DMEM for 24 hours at 37°C . All combinations of materials at different concentrations and crosslinking approaches are summarized in Table S1.

Hydrogels mechanical characterization:

Each sample type was analyzed in terms of Young's modulus (E), fracture stress, fracture strain and toughness. Uniaxial compression was performed with a Instron Mechanical Testing System (model 2444, Instron, Norwood, MA, USA) equipped with both ± 10 N and ± 1000 N load cells at a compression rate of 1 mm min^{-1} until reaching the hydrogel breaking point. E derived from the linear region of the stress-strain curve (the first 10% of strain), fitted according to the equations:

$$\sigma = \frac{F}{A_0} \quad (8)$$

and

$$\varepsilon = \frac{\Delta l}{l_0} \quad (9)$$

where σ and ε are the stress and the strain, F is the force, Δl is the deformation, A_0 is the sample area and l_0 is the sample initial length. E was calculated according to the equation:

$$E = \frac{\sigma}{\varepsilon} \quad (10)$$

The fracture stress and fracture strain were assumed as the stress and strain at which the sample broke. The toughness, defined as the amount of strain energy per unit volume that a hydrogel can absorb, was calculated as the area under the stress-strain curve up to the breaking point.

1 The swelling ratio was assessed to measure the amount of water absorbed by each type of
2 hydrogel. The mass of each sample type was measured after incubation in DMEM for 24 hours
3
4 at room temperature after removing residual liquid using filter paper ($W_{\text{after swelling}}$). Then, each
5
6 sample was dried entirely, and the mass was weighed (W_{dry}). The calculation of swelling ratio
7
8 follows the equation:
9

$$10 \quad SR = \frac{W_{\text{after swelling}}}{W_{\text{dry}}} \quad (11)$$

11 *Graphene oxide synthesis and characterization:*

12 We synthesized GO, as described in our previous paper.^[68] In short, we oxidized graphite flakes
13 using the modified Hummer's method.^[69] A 9:1 mixture of concentrated $\text{H}_2\text{SO}_4/\text{H}_3\text{PO}_4$ (360:40
14 mL) was added to a mixture of graphite flakes (3 g) and KMnO_4 (18 g). The reaction was then
15 heated to 50 °C and stirred for 12 h. Next, the reaction was cooled to room temperature and
16 decanted onto ice (400 mL) with 30% H_2O_2 (3 mL). For workup, the mixture was washed by
17 extensive centrifugation cycles with water (12,000 rpm for 4 h) following by a dialysis for a
18 week. When the solution pH was reached to pH = 7, it was centrifuged again (12,000 rpm for
19 4 h), and finally dried by lyophilization, yielding 5 g of graphite oxide. The obtained graphite
20 oxide (yellowish solid) was exfoliated to GO sheets by half an hour of ultrasonication (brown
21 solution).
22
23
24
25
26
27
28
29
30
31
32
33
34
35
36
37
38
39
40
41

42 The GO bulk was characterized by field-emission SEM (FESEM; FEI, Helios 600) operating
43 at 5 keV. HRTEM measurements were carried out by a JEOL-2100 instrument operating at 200
44 keV. HRTEM samples were prepared by dispersing a section of GO bulk in ethanol followed
45 by a gentle sonication for 15 minutes; then we dropped-cast a single droplet of the dispersion
46 on a 300-mesh Cu lacey carbon grid (from SPI). Raman scattering data in the range of 1000-
47 3000 cm^{-1} was taken using a micro-Raman instrument (HORIBA Scientific LabRAM HR) in
48 the air at RT. GO bulk sample was excited by a laser with an excitation wavelength of $\lambda_{\text{ex}} =$
49 532 nm. AFM measurements were performed by using a Bio FastScan scanning probe
50
51
52
53
54
55
56
57
58
59
60
61
62
63
64
65

1 microscope (Bruker AXS). All images were obtained using soft tapping mode with a Fast Scan
2 B (Bruker) silicon probe (spring constant of 1.8 N/m). The resonance frequency of the
3
4 cantilever was approximately 450 kHz (in the air). The measurements were performed under
5
6 environmental conditions. The images were captured in the retrace direction with a scan rate of
7
8
9 1.6 Hz. The resolution of the images was 512 samples/line. For image processing, we used
10
11 Nanoscope Analysis software. The “flattening” and “plane fit” functions were applied to each
12
13 image. We measured GO flakes on Si/SiO₂ wafer, prepared by a single droplet from the same
14
15 dispersion of GO as before.
16

17 *Preparation of nanocomposite hydrogels:*

18
19
20
21
22
23
24
25
26
27
28
29
30
31
32
33
34
35
36
37
38
39
40
41
42
43
44
45
46
47
48
49
50
51
52
53
54
55
56
57
58
59
60
61
62
63
64
65
66
67
68
69
70
71
72
73
74
75
76
77
78
79
80
81
82
83
84
85
86
87
88
89
90
91
92
93
94
95
96
97
98
99
100
101
102
103
104
105
106
107
108
109
110
111
112
113
114
115
116
117
118
119
120
121
122
123
124
125
126
127
128
129
130
131
132
133
134
135
136
137
138
139
140
141
142
143
144
145
146
147
148
149
150
151
152
153
154
155
156
157
158
159
160
161
162
163
164
165
166
167
168
169
170
171
172
173
174
175
176
177
178
179
180
181
182
183
184
185
186
187
188
189
190
191
192
193
194
195
196
197
198
199
200
201
202
203
204
205
206
207
208
209
210
211
212
213
214
215
216
217
218
219
220
221
222
223
224
225
226
227
228
229
230
231
232
233
234
235
236
237
238
239
240
241
242
243
244
245
246
247
248
249
250
251
252
253
254
255
256
257
258
259
260
261
262
263
264
265
266
267
268
269
270
271
272
273
274
275
276
277
278
279
280
281
282
283
284
285
286
287
288
289
290
291
292
293
294
295
296
297
298
299
300
301
302
303
304
305
306
307
308
309
310
311
312
313
314
315
316
317
318
319
320
321
322
323
324
325
326
327
328
329
330
331
332
333
334
335
336
337
338
339
340
341
342
343
344
345
346
347
348
349
350
351
352
353
354
355
356
357
358
359
360
361
362
363
364
365
366
367
368
369
370
371
372
373
374
375
376
377
378
379
380
381
382
383
384
385
386
387
388
389
390
391
392
393
394
395
396
397
398
399
400
401
402
403
404
405
406
407
408
409
410
411
412
413
414
415
416
417
418
419
420
421
422
423
424
425
426
427
428
429
430
431
432
433
434
435
436
437
438
439
440
441
442
443
444
445
446
447
448
449
450
451
452
453
454
455
456
457
458
459
460
461
462
463
464
465
466
467
468
469
470
471
472
473
474
475
476
477
478
479
480
481
482
483
484
485
486
487
488
489
490
491
492
493
494
495
496
497
498
499
500
501
502
503
504
505
506
507
508
509
510
511
512
513
514
515
516
517
518
519
520
521
522
523
524
525
526
527
528
529
530
531
532
533
534
535
536
537
538
539
540
541
542
543
544
545
546
547
548
549
550
551
552
553
554
555
556
557
558
559
560
561
562
563
564
565
566
567
568
569
570
571
572
573
574
575
576
577
578
579
580
581
582
583
584
585
586
587
588
589
590
591
592
593
594
595
596
597
598
599
600
601
602
603
604
605
606
607
608
609
610
611
612
613
614
615
616
617
618
619
620
621
622
623
624
625
626
627
628
629
630
631
632
633
634
635
636
637
638
639
640
641
642
643
644
645
646
647
648
649
650
651
652
653
654
655
656
657
658
659
660
661
662
663
664
665
666
667
668
669
670
671
672
673
674
675
676
677
678
679
680
681
682
683
684
685
686
687
688
689
690
691
692
693
694
695
696
697
698
699
700
701
702
703
704
705
706
707
708
709
710
711
712
713
714
715
716
717
718
719
720
721
722
723
724
725
726
727
728
729
730
731
732
733
734
735
736
737
738
739
740
741
742
743
744
745
746
747
748
749
750
751
752
753
754
755
756
757
758
759
760
761
762
763
764
765
766
767
768
769
770
771
772
773
774
775
776
777
778
779
780
781
782
783
784
785
786
787
788
789
790
791
792
793
794
795
796
797
798
799
800
801
802
803
804
805
806
807
808
809
810
811
812
813
814
815
816
817
818
819
820
821
822
823
824
825
826
827
828
829
830
831
832
833
834
835
836
837
838
839
840
841
842
843
844
845
846
847
848
849
850
851
852
853
854
855
856
857
858
859
860
861
862
863
864
865
866
867
868
869
870
871
872
873
874
875
876
877
878
879
880
881
882
883
884
885
886
887
888
889
890
891
892
893
894
895
896
897
898
899
900
901
902
903
904
905
906
907
908
909
910
911
912
913
914
915
916
917
918
919
920
921
922
923
924
925
926
927
928
929
930
931
932
933
934
935
936
937
938
939
940
941
942
943
944
945
946
947
948
949
950
951
952
953
954
955
956
957
958
959
960
961
962
963
964
965
966
967
968
969
970
971
972
973
974
975
976
977
978
979
980
981
982
983
984
985
986
987
988
989
990
991
992
993
994
995
996
997
998
999
1000

GO sheets were resuspended in deionized water (0.2 % w/v) and de-agglomerated using an ultrasonic bath (Branson 2510, power: 20 W) for 5 minutes before their use. Then, the GO suspension was added to the GG/PEGDA10_5minUV_10minMgCl₂ hydrogel solution to get a final concentration of 0.01% w/v and the blend (GG/PEGDA10/GO_5minUV_10minMgCl₂) was stirred at 75°C for 30 minutes for obtaining a homogenized solution. After that, the solution was poured into cylindrical holes (diameter: 6 mm; height: 5 mm) of a custom-made PDMS mold and photo-crosslinked upon UV exposure (same parameters described in section 5.2). Later, the ionic crosslinking was performed on some hydrogels by immersing the samples in MgCl₂ solution (1 % w/v in deionized water) for 10 min. Then, the ionic crosslinking was finalized by incubation in DMEM for 24 hours at 37 °C.

A preliminary evaluation of GO nanosheets dispersion in the nanocomposite hydrogel was carried out using an optical microscope (Hirox digital microscope, Hirox Co Ltd.).

51 *Characterization of GO-based nanocomposite hydrogels*

52 *Mechanical characterization:*

53
54
55
56
57
58
59
60
61
62
63
64
65
66
67
68
69
70
71
72
73
74
75
76
77
78
79
80
81
82
83
84
85
86
87
88
89
90
91
92
93
94
95
96
97
98
99
100
101
102
103
104
105
106
107
108
109
110
111
112
113
114
115
116
117
118
119
120
121
122
123
124
125
126
127
128
129
130
131
132
133
134
135
136
137
138
139
140
141
142
143
144
145
146
147
148
149
150
151
152
153
154
155
156
157
158
159
160
161
162
163
164
165
166
167
168
169
170
171
172
173
174
175
176
177
178
179
180
181
182
183
184
185
186
187
188
189
190
191
192
193
194
195
196
197
198
199
200
201
202
203
204
205
206
207
208
209
210
211
212
213
214
215
216
217
218
219
220
221
222
223
224
225
226
227
228
229
230
231
232
233
234
235
236
237
238
239
240
241
242
243
244
245
246
247
248
249
250
251
252
253
254
255
256
257
258
259
260
261
262
263
264
265
266
267
268
269
270
271
272
273
274
275
276
277
278
279
280
281
282
283
284
285
286
287
288
289
290
291
292
293
294
295
296
297
298
299
300
301
302
303
304
305
306
307
308
309
310
311
312
313
314
315
316
317
318
319
320
321
322
323
324
325
326
327
328
329
330
331
332
333
334
335
336
337
338
339
340
341
342
343
344
345
346
347
348
349
350
351
352
353
354
355
356
357
358
359
360
361
362
363
364
365
366
367
368
369
370
371
372
373
374
375
376
377
378
379
380
381
382
383
384
385
386
387
388
389
390
391
392
393
394
395
396
397
398
399
400
401
402
403
404
405
406
407
408
409
410
411
412
413
414
415
416
417
418
419
420
421
422
423
424
425
426
427
428
429
430
431
432
433
434
435
436
437
438
439
440
441
442
443
444
445
446
447
448
449
450
451
452
453
454
455
456
457
458
459
460
461
462
463
464
465
466
467
468
469
470
471
472
473
474
475
476
477
478
479
480
481
482
483
484
485
486
487
488
489
490
491
492
493
494
495
496
497
498
499
500
501
502
503
504
505
506
507
508
509
510
511
512
513
514
515
516
517
518
519
520
521
522
523
524
525
526
527
528
529
530
531
532
533
534
535
536
537
538
539
540
541
542
543
544
545
546
547
548
549
550
551
552
553
554
555
556
557
558
559
560
561
562
563
564
565
566
567
568
569
570
571
572
573
574
575
576
577
578
579
580
581
582
583
584
585
586
587
588
589
590
591
592
593
594
595
596
597
598
599
600
601
602
603
604
605
606
607
608
609
610
611
612
613
614
615
616
617
618
619
620
621
622
623
624
625
626
627
628
629
630
631
632
633
634
635
636
637
638
639
640
641
642
643
644
645
646
647
648
649
650
651
652
653
654
655
656
657
658
659
660
661
662
663
664
665
666
667
668
669
670
671
672
673
674
675
676
677
678
679
680
681
682
683
684
685
686
687
688
689
690
691
692
693
694
695
696
697
698
699
700
701
702
703
704
705
706
707
708
709
710
711
712
713
714
715
716
717
718
719
720
721
722
723
724
725
726
727
728
729
730
731
732
733
734
735
736
737
738
739
740
741
742
743
744
745
746
747
748
749
750
751
752
753
754
755
756
757
758
759
760
761
762
763
764
765
766
767
768
769
770
771
772
773
774
775
776
777
778
779
780
781
782
783
784
785
786
787
788
789
790
791
792
793
794
795
796
797
798
799
800
801
802
803
804
805
806
807
808
809
810
811
812
813
814
815
816
817
818
819
820
821
822
823
824
825
826
827
828
829
830
831
832
833
834
835
836
837
838
839
840
841
842
843
844
845
846
847
848
849
850
851
852
853
854
855
856
857
858
859
860
861
862
863
864
865
866
867
868
869
870
871
872
873
874
875
876
877
878
879
880
881
882
883
884
885
886
887
888
889
890
891
892
893
894
895
896
897
898
899
900
901
902
903
904
905
906
907
908
909
910
911
912
913
914
915
916
917
918
919
920
921
922
923
924
925
926
927
928
929
930
931
932
933
934
935
936
937
938
939
940
941
942
943
944
945
946
947
948
949
950
951
952
953
954
955
956
957
958
959
960
961
962
963
964
965
966
967
968
969
970
971
972
973
974
975
976
977
978
979
980
981
982
983
984
985
986
987
988
989
990
991
992
993
994
995
996
997
998
999
1000

Young's modulus, fracture stress, fracture strain and toughness and swelling ratio were measured as described in section “Hydrogels mechanical characterization”.

Tribological test:

1
2 Tribological tests on crosslinked hydrogels with (GG/PEGDA10/GO_5minUV_10minMgCl₂)
3
4 and without GO (GG/PEGDA10_5minUV_10minMgCl₂) (Figure 4a) were performed using a
5
6 MCR 102 rheometer (Anton Paar) equipped with the Tribocell T-PTD200 and a Peltier
7
8 temperature control, the H-PTD200 hood and a disposable measuring system shaft. Customized
9
10 sample holders were used to keep fixed the specimens on the top of the Tribocell. The test
11
12 geometry was set as flat-on-flat, in which a glass disc mounted on the shaft was interfaced to
13
14 the surface of the hydrogel while lubricating the contact between these components with PBS.
15
16
17 A representation of the tribological set-up is reported in Figure 4b. The glass disc was pressed
18
19 against the sample by applying a normal force of 0.5 N. The torque was measured to realize the
20
21 defined rotational speeds. During all experiments, the temperature was kept constant at 25°C.
22
23

24
25
26 The test was divided into three parts:

- 27
28 1) The normal force was applied and remained constant ($F_N = 0.5$ N) during the entire test. The
29
30 time for adjusting the normal force was kept short (1.5 minutes) to avoid potential evaporation
31
32 of the PBS buffer.
33
34
- 35
36 2) The first and second extended Stribeck curve runs were for running-in. The rotational speed
37
38 was increased logarithmically from 10^{-5} min⁻¹ to 1 min⁻¹. Therefore, the third run was used for
39
40 the final evaluation.
41
42
- 43
44 3) The wear behavior was investigated at a constant rotation speed ($V_s = 5$ mm s⁻¹) for 30
45
46 minutes.
47

48
49 Subsequently, the speed was lowered again. Finally, the COF versus rotational speed and
50
51 torque/thickness versus time were graphed. The COF was determined as the ratio between the
52
53 frictional force and the normal force. Several tests consisted of three consecutive runs each
54
55 were performed.
56

Development of bilayered hydrogels

Preparation of the bilayered structure:

1
2 Bilayered structures were fabricated using the custom-made PDMS mold (diameter: 6 mm;
3
4 height: 5 mm), assuming the volumetric ratios defined into the modeling. Firstly, 113 μl of
5
6 GG/PEGDA15_5minUV_10minMgCl₂ hydrogel solution was poured in the mold to achieve a
7
8 height of 4 mm. Then, the hydrogel solution was photo-crosslinked upon UV light exposure for
9
10 5 minutes and after immersed in MgCl₂ solution (1% w/v, in deionized water) for 10 minutes.
11
12 Subsequently, 28 μl of the nanocomposite GG/PEGDA10/GO_5minUV_10minMgCl₂ was
13
14 poured onto the crosslinked DC layer to achieve a final height of 5 mm. Then, the bilayer was
15
16 photo-crosslinked upon UV light exposure for 5 minutes and after immersed in MgCl₂ solution
17
18 (1% w/v, in deionized water) for 10 minutes. Finally, the crosslinked bilayered structures were
19
20 incubated for 24 hours at RO in DMEM.
21
22
23
24
25

Characterization of bilayered structures:

26
27
28 Young's modulus, fracture stress and strain and toughness were measured after preparation, as
29
30 previously described in section 5.3. The degradation of the bilayered structures was evaluated
31
32 by incubating each sample at 37 °C in PBS (1X) and H₂O₂ (3 % in PBS), according to the
33
34 ISO10993-13, within an orbital agitator (711CT, Elettrofor).^[70] A cyclic agitation at 2 rpm was
35
36 imposed for the whole testing period. The material degradation kinetics was evaluated by
37
38 monitoring the percentage of dry weight loss over time, after 2 weeks and 1 month. Four
39
40 independent samples for each material type were tested.
41
42
43
44

45
46 The mechanical performance of the bilayered structures was also analyzed after 1 month of
47
48 degradation in PBS and H₂O₂ and compared to those owned by the material without being
49
50 subjected to degradation.
51
52

Wear test:

53
54
55 Wear test was carried out to qualitatively evaluate whether the construct remained intact under
56
57 repeated cyclical stresses. In particular, the wear test was performed using a four-station
58
59
60
61

1 displacement control knee joint simulator (Shore Western, Inc., Monrovia, CA, USA) that
2 consents to simulate the knee movement up to four degree-of-freedom (DOF), as previously
3 reported.^[60] Briefly, the menisci were sterilized with ethylene oxide (ETO) gas and tested in
4
5 conjunction with four CoCrMo alloy femoral and tibial components (size 2; Adler ORTHO,
6
7 Milan, Italy), consolidated by compression molding (accordingly to ISO 5834/1-2) and ETO
8
9 sterilized. Four bilayered structures were prepared keeping the same volumetric ratio as
10
11 described previously into two symmetric holes (diameter: 12 mm; height: 7 mm) created into
12
13 Ultra-High-Molecular-Weight-Poly-Ethylene (UHMWPE) mobile menisci (Genus mobile
14
15 bearing, size 2, Adler ORTHO, Milan, Italy). Axial load was applied vertically (perpendicular
16
17 to the tibial tray), oscillating between 168 and 2600 N following the calculated profile. The
18
19 applied kinematics was derived from the displacement control simulator. In particular, the
20
21 flexion/extension angle oscillating between 0° (neutral) and 60° (flexion) was synchronously
22
23 with the load; the anterior/posterior translation oscillating between -6.0 mm (neutral) and 6.0
24
25 mm (posterior), and the intra/extra-rotation oscillating between -2.0° (extra-rotation) and 6.0°
26
27 (intra-rotation). The test was performed using fetal bovine calf serum as a medium and using a
28
29 frequency of 1.0 ± 0.1 Hz, following the ISO 14243. Each test was performed in the presence
30
31 of 25% sterile FBS balanced with deionized water and 0.2% NaN₃ to slow down bacterial
32
33 growth, and 20 mM EDTA to minimize precipitation of calcium phosphate. The wear test lasted
34
35 100.000 cycles. Macroscopic and brightfield (4x) images of all pre-tested and tested sample
36
37 was captured using a professional camera and optical microscope (Nikon 90i, Nikon, Japan).
38
39 The brightfield images of medial and lateral condyles were captured in the center and on the
40
41 edge of samples using an optical microscope.
42
43
44
45
46
47
48
49
50

51 An optical profiler (Leica DCM8) was used to analyze the roughness of the bilayered hydrogels
52
53 in the hydrated state before and after the wear test. Z-stacks (scan area $640 \times 480 \mu\text{m}^2$) were
54
55 acquired, then data were converted into 2D images provided with a height-related greyscale and
56
57
58
59
60
61
62
63
64
65

1 the surface roughness was estimated. The analysis was carried out by using the Gwyddion
2 software (<http://gwyddion.net/>). The average roughness (Ra) was measured on the acquired
3 images. Three Z-stacks were acquired for each sample type in its medial and lateral condyles.
4
5

6 *Cytotoxicity evaluations:*

7
8 To perform *in vitro* cytotoxicity tests, the selected crosslinked
9 GG/PEGDA15_5minUV_10minMgCl₂ and GG/PEGDA10/GO_5minUV_10minMgCl₂
10 hydrogels were incubated for 24 hours in cell culture medium composed of DMEM with 10 %
11 FBS and 100 U/mL penicillin/streptomycin (3 mL/sample). The supernatants were collected
12 and used for the analysis of the cell behavior for the following assays.
13
14

15 Isolated human OA chondrocytes (from male, 59 years old) collected into the biobank of
16 Laboratory of Immunorheumatology and Tissue Regeneration (at Istituto Ortopedico Rizzoli)
17 were thawed and expanded in culture. Chondrocytes at passage 3 were seeded in 8 wells-
18 chamber slides at a cell density of 1.2×10^4 cells/well. Cells were left to adhere for 24 hours,
19 then the culture medium was removed, and the supernatants collected from the
20 GG/PEGDA15_5minUV_10minMgCl₂ and GG/PEGDA10/GO_5minUV_10minMgCl₂
21 hydrogels (500 μ l/well) were transferred on the chamber slides. An untreated control was
22 performed by simply changing the cell culture medium (DMEM, 10% FBS, 100 U/ml
23 penicillin/streptomycin).
24
25

26 Cell morphology and viability were evaluated after 2 and 6 days by Live/Dead[®] cell viability
27 assay.^[71] Cells were washed twice with PBS and then incubated with Ethidium homodimer-1
28 (4 μ M) and Calcein AM (2 μ M) for 45 minutes at 37°C and 5% CO₂. Labeled cells were then
29 visualized under an optical microscope (Nikon, Japan) for evaluating general morphology,
30 viable (green) and dead (red) cells.
31
32

33 The MTT metabolic activity assay determined the ability of viable cells to reduce the yellow
34 tetrazolium salt (MTT) to blue-colored formazan crystals by mitochondrial enzymes, detectable
35
36

1 with a spectrophotometer. MTT metabolic activity assay was performed at the same time points
2 (2 and 6 days). Cells were washed twice with PBS and then incubated with MTT for 3 hours at
3
4 37°C and 5% CO₂. Afterward, MTT solution was removed and HCl (0.1 M) was added to cells
5
6 to permit redox reaction in formazan. Absorbance at 570 nm was evaluated using a
7
8 spectrophotometer (Tecan, Life Science).
9
10

11 **Statistical analysis:**

12
13
14
15
16 Normality tests (D'Agostino-Pearson) were performed on all experimental data to assess the
17
18 type of data distribution. Results with normal distribution were expressed as average values ±
19
20 standard deviations. Data analysis was performed by applying the Student's t-tests to evaluate
21
22 statistically significant differences between two sample types under analysis, while one-way
23
24 ANOVA with Tukey's post-test was adopted for multiple comparisons. Statistical analysis was
25
26 carried out using GraphPad Prism (v 6.0). The significance threshold was set at 5% (* p < 0.05)
27
28 and 1% (** p < 0.01).
29
30
31
32
33
34
35

36 **Supporting Information**

37 Supporting Information is available from the Wiley Online Library or from the author.
38
39
40

41 **Acknowledgements**

42 This work received funding from the European Union's Horizon 2020 research and innovation
43 program, grant agreement No 814413, project ADMAIORA (Advanced nano composite
44 MAterials fOr in situ treatment and ultRASound-mediated management of osteoarthritis).
45
46

47 Received: ((will be filled in by the editorial staff))

48 Revised: ((will be filled in by the editorial staff))

49 Published online: ((will be filled in by the editorial staff))
50
51
52

53 **References**

- 54
55
56 [1] L. M. Anthony, LANGE Series, McGraw-Hill Medical, 2013.
57 [2] a) A. J. Sophia Fox, A. Bedi, S. A. Rodeo, *Sports Health* **2009**, 1, 461; b) C. B.
58 Carballo, Y. Nakagawa, I. Sekiya, S. A. Rodeo, *Clin Sports Med* **2017**, 36, 413.
59
60
61
62
63
64
65

- [3] J. Antons, M. G. M. Marascio, J. Nohava, R. Martin, L. A. Applegate, P. E. Bourban, D. P. Pioletti, *Journal of Materials Science: Materials in Medicine* **2018**, 29, 57.
- [4] B. He, J. P. Wu, T. B. Kirk, J. A. Carrino, C. Xiang, J. Xu, *Arthritis Research & Therapy* **2014**, 16, 205.
- [5] J. S. Jurvelin, M. D. Buschmann, E. B. Hunziker, *Proceedings of the Institution of Mechanical Engineers, Part H: Journal of Engineering in Medicine* **2003**, 217, 215.
- [6] a) R. Krishnan, S. Park, F. Eckstein, G. A. Ateshian, *Journal of Biomechanical Engineering* **2003**, 125, 569; b) G. O'Connell, J. Garcia, J. Amir, *ACS Biomaterials Science & Engineering* **2017**, 3, 2657.
- [7] S. Camarero-Espinosa, B. Rothen-Rutishauser, E. J. Foster, C. Weder, *Biomaterials Science* **2016**, 4, 734.
- [8] K.-X. A. L. Hooi Yee Ng, Yu-Fang Shen, *JSM Bone and Joint Dis* **2017**, 1(2): 1010.
- [9] a) D. J. Hunter, S. Bierma-Zeinstra, *Lancet* **2019**, 393, 1745; b) L. A. McMahon, F. J. O'Brien, P. J. Prendergast, *Regen Med* **2008**, 3, 743; c) L. Zhang, J. Hu, K. A. Athanasiou, *Critical reviews in biomedical engineering* **2009**, 37, 1.
- [10] M. A. Jeffries, *Osteoarthritis Cartilage* **2019**, 27, 371.
- [11] A. D. Pearle, R. F. Warren, S. A. Rodeo, *Clinics in Sports Medicine* **2005**, 24, 1.
- [12] a) J. A. Buckwalter, *A Publication of The Association of Bone and Joint Surgeons® / CORR®* **2002**, 402; b) A. E. Peters, R. Akhtar, E. J. Comerford, K. T. Bates, *Scientific Reports* **2018**, 8, 5931.
- [13] S. G. Walter, R. Ossendorff, F. A. Schildberg, *Archives of Orthopaedic and Trauma Surgery* **2019**, 139, 305.
- [14] a) E. T. Hurley, C. D. Murawski, J. Paul, A. Marangon, M. P. Prado, X. Xu, L. Hangody, J. G. Kennedy, *Foot Ankle Int* **2018**, 39, 28s; b) A. Ng, K. Bernhard, *Clin Podiatr Med Surg* **2017**, 34, 461; c) S. L. Sherman, E. Thyssen, C. W. Nuelle, *Clinics in Sports Medicine* **2017**, 36, 489.
- [15] S. Elder, H. Chenault, P. Gloth, K. Webb, R. Recinos, E. Wright, D. Moran, J. Butler, A. Borazjani, A. Cooley, *J Biomed Mater Res A* **2018**, 106, 2251.
- [16] a) K. P. Krafts, *Organogenesis* **2010**, 6, 225; b) M. A. Heinrich, W. Liu, A. Jimenez, J. Yang, A. Akpek, X. Liu, Q. Pi, X. Mu, N. Hu, R. M. Schiffelers, J. Prakash, J. Xie, Y. S. Zhang, *Small* **2019**, 15, e1805510; c) M. Zeng, S. Jin, K. Ye, *SLAS Technol* **2018**, DOI: 10.1177/24726303187605152472630318760515.
- [17] H. Kwon, W. E. Brown, C. A. Lee, D. Wang, N. Paschos, J. C. Hu, K. A. Athanasiou, *Nat Rev Rheumatol* **2019**, 15, 550.
- [18] L. Cipollaro, M. C. Ciardulli, G. D. Porta, G. M. Peretti, N. Maffulli, *British Medical Bulletin* **2019**, 132, 53.
- [19] a) X. Zhou, T. Esworthy, S. J. Lee, S. Miao, H. Cui, M. Plesiniak, H. Fenniri, T. Webster, R. D. Rao, L. G. Zhang, *Nanomedicine* **2019**, 19, 58; b) J. Idaszek, M. Costantini, T. A. Karlsen, J. Jaroszewicz, C. Colosi, S. Testa, E. Fornetti, S. Bernardini, M. Seta, K. Kasarełło, R. Wrzesień, S. Cannata, A. Barbeta, C. Gargioli, J. E. Brinchman, W. Świążkowski, *Biofabrication* **2019**, 11, 044101; c) L. Costa, J. Silva-Correia, J. M. Oliveira, R. L. Reis, in *Osteochondral Tissue Engineering: Nanotechnology, Scaffolding-Related Developments and Translation*, DOI: 10.1007/978-3-319-76711-6_13 (Eds: J. M. Oliveira, S. Pina, R. L. Reis, J. San Roman), Springer International Publishing, Cham **2018**, p. 281; d) S. Zhang, L. Chen, Y. Jiang, Y. Cai, G. Xu, T. Tong, W. Zhang, L. Wang, J. Ji, P. Shi, H. W. Ouyang, *Acta Biomater* **2013**, 9, 7236; e) E. J. Sheehy, T. Vinardell, C. T. Buckley, D. J. Kelly, *Acta Biomater* **2013**, 9, 5484; f) K. Kim, J. Lam, S. Lu, P. P. Spicer, A. Lueckgen, Y. Tabata, M. E. Wong, J. A. Jansen, A. G. Mikos, F. K. Kasper, *J Control Release* **2013**, 168, 166; g) S. Jin-Hyung, L. Jung-Seob, K. Jong Young, C. Dong-Woo, *Journal of*

- Micromechanics and Microengineering* **2012**, 22, 085014; h) Z. Jia, F. Zhu, X. Li, Q. Liang, Z. Zhuo, J. Huang, L. Duan, J. Xiong, D. Wang, *Mater Sci Eng C Mater Biol Appl* **2019**, 99, 541.
- [20] C. Gegg, F. Yang, *Acta Biomaterialia* **2020**, 101, 196.
- [21] L. Jiang, Y. Wang, Z. Liu, C. Ma, H. Yan, N. Xu, F. Gang, X. M. Wang, L. Zhao, X. Sun, *Tissue Eng Part B Rev* **2019**, DOI: 10.1089/ten.TEB.2019.0100.
- [22] S. D. Eswaramoorthy, S. Ramakrishna, S. N. Rath, *J Tissue Eng Regen Med* **2019**, DOI: 10.1002/term.2839.
- [23] H. Chen, A. d. B. F. B. Malheiro, C. van Blitterswijk, C. Mota, P. A. Wieringa, L. Moroni, *ACS Applied Materials & Interfaces* **2017**, 9, 38187.
- [24] a) J. A. M. Steele, S. D. McCullen, A. Callanan, H. Autefage, M. A. Accardi, D. Dini, M. M. Stevens, *Acta Biomaterialia* **2014**, 10, 2065; b) M. Castilho, V. Mouser, M. Chen, J. Malda, K. Ito, *Acta Biomaterialia* **2019**, 95, 297.
- [25] X. Ren, F. Wang, C. Chen, X. Gong, L. Yin, L. Yang, *BMC Musculoskeletal Disorders* **2016**, 17, 301.
- [26] J. T. Oliveira, L. Martins, R. Picciochi, P. B. Malafaya, R. A. Sousa, N. M. Neves, J. F. Mano, R. L. Reis, *Journal of Biomedical Materials Research Part A* **2010**, 93A, 852.
- [27] a) D. F. Coutinho, S. V. Sant, H. Shin, J. T. Oliveira, M. E. Gomes, N. M. Neves, A. Khademhosseini, R. L. Reis, *Biomaterials* **2010**, 31, 7494; b) J. Silva-Correia, J. M. Oliveira, S. G. Caridade, J. T. Oliveira, R. A. Sousa, J. F. Mano, R. L. Reis, *Journal of Tissue Engineering and Regenerative Medicine* **2011**, 5, e97.
- [28] Y. Zhang, J. Xu, Y. Qu, X. Xi, J. Yang, *Ceramics International* **2014**, 40, 5715.
- [29] a) S. Lee, J. H. Choi, A. Park, M. Rim, J. Youn, W. Lee, J. E. Song, G. Khang, *International Journal of Biological Macromolecules* **2020**, 158, 452; b) T.-R. Kim, M.-S. Kim, S. T. Goh, S. J. Lee, H. Y. Kim, S.-Y. Yoon, C.-S. Lee, *Applied Sciences* **2019**, 9.
- [30] Q. T. Nguyen, Y. Hwang, A. C. Chen, S. Varghese, R. L. Sah, *Biomaterials* **2012**, 33, 6682.
- [31] a) W. C. Lee, C. H. Lim, Kenry, C. Su, K. P. Loh, C. T. Lim, *Small* **2015**, 11, 963; b) J. Liao, Y. Qu, B. Chu, X. Zhang, Z. Qian, *Scientific Reports* **2015**, 5, 9879.
- [32] H. Liang, Y. Bu, J. Zhang, *ACS Applied Materials & Interfaces* **2013**, 5, 6369.
- [33] Y. Xin, T. Li, D. Gong, F. Xu, M. Wang, *RSC Advances* **2017**, 7, 6323.
- [34] M. A. Bonifacio, P. Gentile, A. M. Ferreira, S. Cometa, E. De Giglio, *Carbohydrate Polymers* **2017**, 163, 280.
- [35] L. Vannozzi, I. C. Yasa, H. Ceylan, A. Mencias, L. Ricotti, M. Sitti, *Macromolecular Bioscience* **2018**, 18, 1700377.
- [36] D. Wu, Y. Yu, J. Tan, L. Huang, B. Luo, L. Lu, C. Zhou, *Materials & Design* **2018**, 160, 486.
- [37] H. Yao, J. K. Xu, N. Y. Zheng, J. L. Wang, S. W. Mok, Y. W. Lee, L. Shi, J. Y. Wang, J. Yue, S. H. Yung, P. J. Hu, Y. C. Ruan, Y. F. Zhang, K. W. Ho, L. Qin, *Osteoarthritis and Cartilage* **2019**, 27, 1811.
- [38] F. Ma, Y. Ge, N. Liu, X. Pang, X. Shen, B. Tang, *Journal of Materials Chemistry B* **2019**, 7, 2463.
- [39] Q. Chen, D. Wei, H. Chen, L. Zhu, C. Jiao, G. Liu, L. Huang, J. Yang, L. Wang, J. Zheng, *Macromolecules* **2015**, 48, 8003.
- [40] A. K. Means, C. S. Shrode, L. V. Whitney, D. A. Ehrhardt, M. A. Grunlan, *Biomacromolecules* **2019**, 20, 2034.
- [41] D. Kang, Z. Cai, Q. Jin, H. Zhang, *Carbon* **2015**, 91, 445.

- [42] a) S. Mun, H. C. Kim, M. Yadave, J. Kim, *Composite Interfaces* **2015**, 22, 249; b) S. M. Zargar, M. Mehdikhani, M. Rafienia, *Journal of Bioactive and Compatible Polymers* **2019**, 34, 331.
- [43] D. C. Marcano, D. V. Kosynkin, J. M. Berlin, A. Sinitskii, Z. Sun, A. Slesarev, L. B. Alemany, W. Lu, J. M. Tour, *ACS Nano* **2010**, 4, 4806.
- [44] K. Sood, J. Kaur, H. Singh, S. Kumar Arya, M. Khatri, *Toxicology Reports* **2019**, 6, 768.
- [45] X. Zhou, M. Nowicki, H. Cui, W. Zhu, X. Fang, S. Miao, S.-J. Lee, M. Keidar, L. G. Zhang, *Carbon* **2017**, 116, 615.
- [46] J. Wang, J. Qiao, J. Wang, Y. Zhu, L. Jiang, *ACS Applied Materials & Interfaces* **2015**, 7, 9281.
- [47] a) R. Balu, S. Reeder, R. Knott, J. Mata, L. de Campo, N. K. Dutta, N. R. Choudhury, *Langmuir* **2018**, 34, 9238; b) Y. Meng, L. Ye, P. Coates, P. Twigg, *The Journal of Physical Chemistry C* **2018**, 122, 3157.
- [48] a) C. Cha, S. R. Shin, X. Gao, N. Annabi, M. R. Dokmeci, X. Tang, A. Khademhosseini, *Small* **2014**, 10, 514; b) R. Liu, S. Liang, X.-Z. Tang, D. Yan, X. Li, Z.-Z. Yu, *Journal of Materials Chemistry* **2012**, 22, 14160.
- [49] J. P. Gleghorn, L. J. Bonassar, *Journal of Biomechanics* **2008**, 41, 1910.
- [50] X. Gao, P. Ju, X. Liu, L. Chen, L. Ji, H. Li, H. Zhou, J. Chen, *Industrial & Engineering Chemistry Research* **2019**, 58, 5464.
- [51] J. Tang, S. Chen, Y. Jia, Y. Ma, H. Xie, X. Quan, Q. Ding, *Carbon* **2020**, 156, 272.
- [52] Z. J. Zhang, D. Simionesie, C. Schaschke, *Lubricants* **2014**, 2.
- [53] a) S. M. McNary, K. A. Athanasiou, A. H. Reddi, *Tissue Engineering Part B: Reviews* **2011**, 18, 88; b) P. E. Milner, M. Parkes, J. L. Puetzer, R. Chapman, M. M. Stevens, P. Cann, J. R. T. Jeffers, *Acta Biomaterialia* **2018**, 65, 102; c) B. Wang, W. Tang, H. Lu, Z. Huang, *Journal of Materials Chemistry A* **2016**, 4, 7257.
- [54] L. V. Gibiansky, R. Lakes, *Mechanics of Materials* **1997**, 25, 79.
- [55] F. Boschetti, G. Pennati, F. Gervaso, G. M. Peretti, G. Dubini, *Biorheology* **2004**, 41, 159.
- [56] G. Pattappa, B. Johnstone, J. Zellner, D. Docheva, P. Angele, *International Journal of Molecular Sciences* **2019**, 20.
- [57] a) W. Zhao, X. Li, S. Gao, Y. Feng, J. Huang, *Cellulose* **2017**, 24, 2095; b) J. Cui, M. A. Lackey, G. N. Tew, A. J. Crosby, *Macromolecules* **2012**, 45, 6104; c) J. Hu, T. Kurokawa, K. Hiwatashi, T. Nakajima, Z. L. Wu, S. M. Liang, J. P. Gong, *Macromolecules* **2012**, 45, 5218; d) C. W. Peak, J. J. Wilker, G. Schmidt, *Colloid and Polymer Science* **2013**, 291, 2031.
- [58] D. K. Dempsey, C. Carranza, C. P. Chawla, P. Gray, J. H. Eoh, S. Cereceres, E. M. Cosgriff-Hernandez, *Journal of Biomedical Materials Research Part A* **2014**, 102, 3649.
- [59] L. Li, K. Zhang, T. Wang, P. Wang, B. Xue, Y. Cao, L. Zhu, Q. Jiang, *Materials & Design* **2020**, 189, 108492.
- [60] S. Abdel-Jaber, C. Belvedere, A. Leardini, S. Affatato, *Journal of Biomechanics* **2015**, 48, 3830.
- [61] A. J. S. Fox, A. Bedi, S. A. Rodeo, *Sports health* **2012**, 4, 340.
- [62] K. J. Vazquez, J. T. Andreae, C. R. Henak, *J Mech Behav Biomed Mater* **2019**, 98, 262.
- [63] C. Di Bella, S. Duchi, C. D. O'Connell, R. Blanchard, C. Augustine, Z. Yue, F. Thompson, C. Richards, S. Beirne, C. Onofrillo, S. H. Bauquier, S. D. Ryan, P. Pivonka, G. G. Wallace, P. F. Choong, *J Tissue Eng Regen Med* **2018**, 12, 611.

- 1 [64] S. C. Shelmerdine, I. C. Simcock, J. C. Hutchinson, R. Aughwane, A. Melbourne, D.
2 I. Nikitichev, J. L. Ong, A. Borghi, G. Cole, E. Kingham, A. D. Calder, C. Capelli, A.
3 Akhtar, A. C. Cook, S. Schievano, A. David, S. Ourselin, N. J. Sebire, O. J. Arthurs,
4 *The British journal of radiology* **2018**, 91, 20180306.
- 5 [65] P. Kumar, A. Nagarajan, P. D. Uchil, *Cold Spring Harb Protoc* **2018**, 2018.
- 6 [66] W. Li, D. Wu, D. Hu, S. Zhu, C. Pan, Y. Jiao, L. Li, B. Luo, C. Zhou, L. Lu, *Materials*
7 *Science and Engineering: C* **2020**, 107, 110333.
- 8 [67] C. Modroga, A. M. Pandele, C. Bobiričă, D. Dobrotă, A. M. Dăncilă, G. Gârleanu,
9 O. D. Orbuleț, C. Borda, D. Gârleanu, C. Orbeci, *Polymers* **2020**, 12.
- 10 [68] O. Marciano, S. Gonen, N. Levy, E. Teblum, R. Yemini, G. D. Nessim, S. Ruthstein,
11 L. Elbaz, *Langmuir* **2016**, 32, 11672.
- 12 [69] D. C. Marcano, D. V. Kosynkin, J. M. Berlin, A. Sinitskii, Z. Sun, A. Slesarev, L. B.
13 Alemany, W. Lu, J. M. Tour, *Acs Nano* **2010**, 4, 4806.
- 14 [70] A. Cafarelli, P. Losi, A. R. Salgarella, M. C. Barsotti, I. B. Di Cioccio, I. Foffa, L.
15 Vannozzi, P. Pingue, G. Soldani, L. Ricotti, *Journal of the Mechanical Behavior of*
16 *Biomedical Materials* **2019**, 97, 138.
- 17 [71] A. Sharma, G. Desando, M. Petretta, S. Chawla, I. Bartolotti, C. Manferdini, F.
18 Paolella, E. Gabusi, D. Trucco, S. Ghosh, G. Lisignoli, *ACS Biomaterials Science &*
19 *Engineering* **2019**, DOI: 10.1021/acsbiomaterials.8b01631.
20
21
22
23
24
25
26
27
28
29
30
31
32
33
34
35
36
37
38
39
40
41
42
43
44
45
46
47
48
49
50
51
52
53
54
55
56
57
58
59
60
61
62
63
64
65

Supporting Information

Graphene Oxide-doped Gellan Gum-PEGDA hydrogel mimicking the mechanical and lubrication properties of articular cartilage

Diego Trucco^{†,*}, Lorenzo Vannozzi[†], Eti Teblum, Madina Telkhozhayeva, Gilbert Daniel Nessim, Saverio Affatato, Hind Al-Haddad, Gina Lisignoli[§] and Leonardo Ricotti[§]

D. Trucco, Dr. L. Vannozzi, Hind Al-Haddad, Prof. L. Ricotti
The BioRobotics Institute, Scuola Superiore Sant'Anna,
Piazza Martiri della Libertà 33, 56127 Pisa, Italy

Department of Excellence in Robotics & AI, Scuola Superiore Sant'Anna,
Piazza Martiri della Libertà 33, 56127 Pisa, Italy

E-mail: diego.trucco@santannapisa.it

E-mail: leonardo.ricotti@santannapisa.it

D. Trucco, Dr. G. Lisignoli
IRCSS Istituto Ortopedico Rizzoli,
SC Laboratorio di Immunoreumatologia e Rigenerazione Tissutale,
Via di Barbiano, 1/10, Bologna 40136, Italy
E-mail: gina.lisignoli@ior.it

Dr. E. Teblum, M. Telkhozhayeva, Prof. Gilbert D. Nessim,
Department of Chemistry, Bar-Ilan University,
Ramat Gan 52900, Israel

Bar Ilan Institute for Nanotechnology and Advanced Materials (BINA),
Bar-Ilan University, Ramat Gan 52900, Israel

Dr. S. Affatato
IRCSS Istituto Ortopedico Rizzoli,
Laboratorio Tecnologie Biomediche,
Via di Barbiano, 1/10, Bologna 40136, Italy

[†] equally contributing authors

* Corresponding Author

[§] Co-corresponding Authors

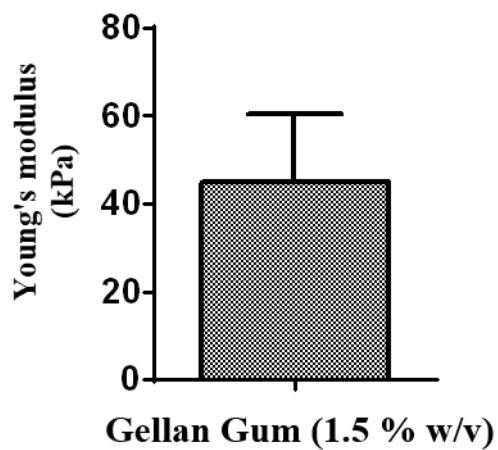


Figure S1. Young's modulus of Gellan Gum at 1.5 % w/v, ionically crosslinked with MgCl_2 (1 % w/v) for 10 min.

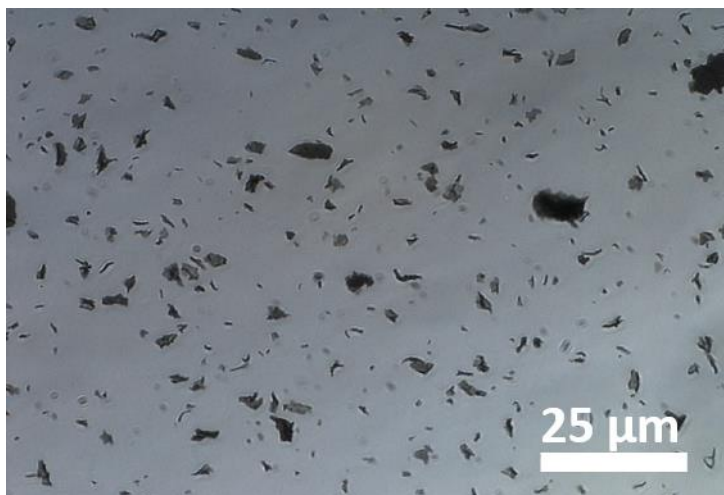


Figure S2. Bright field image of the GG/PEGDA_{10_5minUV_10minMgCl₂} hydrogel with embedded GO.

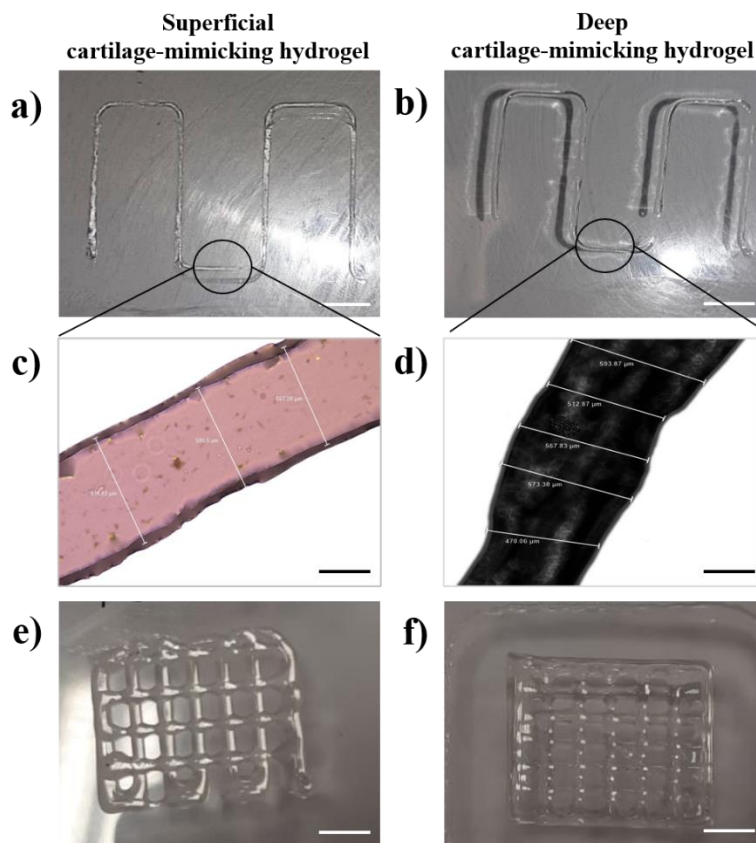


Figure S3. (a-b) Captured images using professional camera (Nikon) performed to evaluate the printed filaments resolution of superficial and deep cartilage-mimicking hydrogels, respectively, using a 22 G needle tip (inner diameter = 410 μm). Scale bars: 5 mm. c-d) Bright field images captured to measure the printed filaments width. Scale bars: 250 μm. The widths were 548.45 ± 7.67 μm and 589.72 ± 20.26 μm for the superficial and deep cartilage-mimicking hydrogels, respectively. e-f) 3D printed structures made of superficial and deep cartilage-mimicking hydrogels. Scale bars: 2 mm.

Table S1. List of the tested formulations.

Experimental groups	GG	PEGDA	GO	I2959	UV exposure	MgCl ₂ incubation	DMEM incubation
GG/PEGDA10_5minUV	1.5 %	10 %	-	0.1 %	5 min	-	24 h
GG/PEGDA10_5minUV_10minMgCl ₂	1.5 %	10 %	-	0.1 %	5 min	10 min	24 h
GG/PEGDA10_10minUV	1.5 %	10 %	-	0.1 %	10 min	-	24 h
GG/PEGDA10_10minUV_10minMgCl ₂	1.5 %	10 %	-	0.1 %	10 min	10 min	24 h
GG/PEGDA15_5minUV	1.5 %	15 %	-	0.1 %	5 min	-	24 h
GG/PEGDA15_5min_10minMgCl ₂	1.5 %	15 %	-	0.1 %	5 min	10 min	24 h
GG/PEGDA15_10minUV	1.5 %	15 %	-	0.1 %	10 min	-	24 h
GG/PEGDA15_10minUV_10minMgCl ₂	1.5 %	15 %	-	0.1 %	10 min	10 min	24 h
GG/PEGDA10/GO_5minUV_10minMgCl ₂	1.5 %	10 %	0.01 %	0.1 %	5 min	10 min	24 h

Movie S1. In the movie, the wear test is shown. The bilayered hydrogel poured into the meniscus-like phantom is stressed by metal knee prosthesis following the ISO 14243. Each simulator's component is shown and described in Figure 6.b.

1
2
3
4
5
6
7
8
9
10
11
12
13
14
15
16
17
18
19
20
21
22
23
24
25
26
27
28
29
30
31
32
33
34
35
36
37
38
39
40
41
42
43
44
45
46
47
48
49
50
51
52
53
54
55
56
57
58
59
60
61
62
63
64
65

Movie S2. In the movie, the preliminary 3D-printability test using 3Dynamic Omega bioprinter is shown. The nanocomposite hydrogel (GG/PEGDA10/GO) was inserted into 20 mL plastic syringe used as cartridges and extruded through a 22 G tip (inner diameter = 410 μm) at room temperature on a Petri dish (150*15 mm) as printing surfaces. The separating distance between the needle and printing surface was set at 3 mm, the layer thickness was kept at 0.3 mm, and the printing speed was set at 25 mm min^{-1} . Repetier-Host and Slic3r software were used to control the printer and printing parameters, respectively.

1
2
3
4
5
6
7
8
9
10
11
12
13
14
15
16
17
18
19
20
21
22
23
24
25
26
27
28
29
30
31
32
33
34
35
36
37
38
39
40
41
42
43
44
45
46
47
48
49
50
51
52
53
54
55
56
57
58
59
60
61
62
63
64
65